Global and Planetary Change 181 (2019) 102989

Contents lists available at ScienceDirect

Global and Planetary Change

journal homepage: www.elsevier.com/locate/gloplacha

Research article

Detection of UHI bias in China climate network using Tmin and Tmax surface temperature divergence

Nicola Scafetta[a,*], Shenghui Ouyang[b]

[a] Department of Earth Sciences, Environment and Georesources, University of Naples Federico II, Via Cinthia 21, 80126 Naples, Italy
[b] MOE Key Laboratory of Surficial Geochemistry, Department of Earth and Planetary Sciences, Nanjing University, Nanjing 210023, China

ARTICLE INFO

Keywords:
China regional temperatures
Urban heat island effects
Global warming
Global climate models
Tmax and Tmin

ABSTRACT

Near-surface temperature records show that China warmed by about 0.8 °C from 1950 to 2010. However, there exists an ongoing debate about whether this warming might have been partially due to urbanization bias. In fact, homogenization approaches may be inefficient in densely populated provinces that have experienced a significant urban development since the 1940s. This paper aims to complement previous research on the topic by showing that an alternative approach based on the analysis of the divergence between the minimum (Tmin) and maximum (Tmax) near-surface temperature records since the 1940s could be useful to clarify the issue because urban heat island (UHI) effects stress the warming of nocturnal temperatures more than the diurnal ones. Then, the significance of the divergence observed in the data could be evaluated against the expectations produced by the CMIP5 general circulation model simulations. From 1945–1954 to 2005–2014, on average and over China, these models predict that Tmin had to warm 0.19 ± 0.06 °C more than Tmax. However, during the same period, the climatic records show that Tmin warmed 0.83 ± 0.15 °C more than Tmax. A similar analysis demonstrates that the effect is more pronounced during the colder months from November–April than during the warmer ones from May to October. A comparison versus China urbanization records demonstrates that the regions characterized by a large Tmin-Tmax divergence are also the most densely populated ones, such as north-east China, that have experienced a diffused and fast urbanization since the 1940s. The results are significant and may indicate the presence of a substantial uncorrected urbanization bias in the Chinese climate records. Under the hypothesis that Tmax is a better metric for studying climatic changes than Tmean or Tmin, we conclude that about 50% of the recorded warming of China since the 1940s could be due to uncorrected urbanization bias. In addition, we also find that the Tmax record from May to October over China shows the 1940s and the 2000s equally warm, in contrast to the 1 °C warming predicted by the CMIP5 models.

1. Introduction

There have been several attempts to estimate surface air temperature trends over China during the last century (Wang et al., 2001, 2004; Tang and Ren, 2005; Tang et al., 2010; Ren et al., 2012, 2017; Cao et al., 2013; Ding et al., 2014; Wang et al., 2014; Soon et al., 2015; Li et al., 2017). The issue is problematic because during the 20th century China has experienced a significant population increase and a very fast and diffused urbanization process, which could have corrupted climatic records because urban heat island (UHI) biases weather station records (Oke, 1987; Stull, 1988; Kershaw, 2017). Thus, it is possible that current estimates of regional Chinese temperature trends since the 1940s might be too high and unrepresentative of the true regional temperature trends.

Homogenization approaches are applied to meteorological temperature records to correct them of any one-off step change biases due to station moves or changes in instrumentation. Several authors argued that the homogenization process indirectly corrects for urbanization bias (Yan et al., 2016; Wang et al., 2017). Others, such as Soon et al. (2018) argued that by itself it leads to urban blending meaning that the magnitude of urbanization bias ends up significantly underestimated. There is also a controversy over the effects of station moves on estimating urbanization bias in China. In recognition of the fact that urban heat islands are not representative of the surrounding countryside, Chinese stations that are becoming highly urbanized, are often moved out to slightly less urbanized areas every few decades. Some groups argue that this means that homogenizing the data for these station moves could reduce the magnitude of the apparent UHI bias (Yan et al.,

* Corresponding author.
E-mail address: nicola.scafetta@unina.it (N. Scafetta).

https://doi.org/10.1016/j.gloplacha.2019.102989
Received 25 February 2019; Received in revised form 1 July 2019; Accepted 12 July 2019
Available online 15 July 2019
0921-8181/

Table 1
Warming between the decades 1945–1954 and 2005–2014 in the CRU temperature records and CMIP5 GCM ensemble mean simulations for the maximum, average and minimum temperature records.

	Tmax (°C)	Tmean (°C)	Tmin. (°C)	Tmin–Tmax (°C)
CRU 4.0 Temp	0.37 ± 0.12	0.79 ± 0.10	1.20 ± 0.08	0.83 ± 0.15
CMIP5 GCM	0.75 ± 0.04	0.84 ± 0.04	0.94 ± 0.04	0.19 ± 0.06

2016). Others argue the exact opposite (e.g.: Ren et al., 2007; Yang et al., 2013). Soon et al. (2018) argue that the main reason for this controversy depends on whether urban blending is adequately avoided.

Therefore, the exact magnitude of the UHI bias in the Chinese climate network has been the subject of considerable debate and there is still a wide range of conflicting opinions. Some argue that urbanization bias is small or even negligible, (e.g.: Li et al., 2004; Li et al., 2010). Some argue that urbanization bias is small after homogenization (e.g.: Yan et al., 2016; Wang et al., 2017). Some argue that urbanization bias is substantial for certain highly urbanized regions such as Beijing (before and after homogenization) (e.g.: Ren et al., 2007; Wang et al., 2013; Yang et al., 2013; Zhang et al., 2014). Some argue that urbanization bias is substantial for the entire network (before and after homogenization) (e.g.: Ren, 2015; Shi et al., 2019 – Table 1 contains a nice summary of the Chinese UHI literature on this topic; Sun et al., 2016; Soon et al., 2018). Soon et al. (2018) pointed out also that, in China, determining how the post-2000 warm period compares against an early 20th-century warm period (occurred around the 1940s) is still controversial. These authors analyzed several climate records including those from five different station subsets collected according to the urbanization degree of their area. They concluded that urban areas (mostly concentrated in east China) and rural areas (mostly concentrated in west China) appear to behave differently. However, an issue remains regarding whether and how much their results may depend on just the different weather patterns characterizing various Chinese regions.

Very few of the Chinese stations are still genuinely rural. Of these few still-rural stations, many of them are often located in climatically distinct regions to the urban stations, e.g., rural mountainous regions versus the more urbanized plains. Moreover, as said above, in recognition of the fact that urban temperatures are unrepresentative of the surrounding countryside, station observers in China occasionally move highly urbanized stations to slightly less urbanized locations every few decades. This makes China a particularly challenging area for estimating the magnitude of the urbanization (warming) bias in the surface air temperature data using conventional approaches. Most of the available data is from stations that are at least partially urbanized. Thus, there is very little rural data for applying the classic urban-minus-rural estimation method.

The very fact that there is such an ongoing debate over the magnitude of UHI bias justifies alternative analyses that could shed new light on the above issue and, possibly, come closer to a solution. The analysis proposed herein takes into account that UHI effects vary according to weather conditions, season, and the time of day (Oke, 1987; Stull, 1988; Kershaw, 2017). Although we may not be the first group to consider the different effects of urbanization on Tmin vs Tmax or even the first to do so for China, what may be considered novel is that we compare these divergences to the equivalent values calculated from the output of the CMIP5 general circulation models hindcasts that provide us with a theoretical expectation of what the observed Tmax-Tmin divergences should have been for China in the absence of non-climatic biases. Thus, by comparing specific climate temperature records versus theoretical predictions it may be possible to better quantify the bias still present in the data and to identify those regions over China where it could be more relevant.

The following step is a comparison against the urbanization development in China since 1950 that could confirm whether the discrepancy observed between theoretical and observed climatic records can be ascribed to uncorrected urbanization biases. The latter should be stronger in the areas that have experienced a faster and more diffused urbanization. Other geographical and climatic constraints could be noted as well. The main purpose of the present research is to correctly evaluate climate change over China during the last century and to appropriately test and evaluate general circulation climate models (GCMs) that are then used to predict future climate change evolutions (cf. Bindoff et al., 2013).

1.1. Urban Heat Island effects and the atmospheric boundary layer physics

UHI is a local warming phenomenon. Higher temperatures occur in urban areas because of their dense concentrations of materials like asphalt, concrete and buildings that absorb more heat during daytime and release it more slowly at night than natural ground cover such as soil and vegetation found in rural areas. For example, by the end of the 20th century, the temperature difference between London and its rural surroundings has been on average about 7 °C (Kershaw, 2017).

Climate studies normally consider temperature anomaly variations from a given 30-year mean period. Thus, in stationary conditions, UHI should not alter climatic averages and trends. However, a warming bias occurs in the data when rural landscapes are slowly converted into urban areas: this transition induces a local increase of the absolute temperatures. Thus, if a meteorological station was once located in an isolated rural area that has been subsequently gradually incorporated into a more urban environment, then the temperature record from that weather station would be affected by an urbanization bias. This bias must be filtered out before compiling the climatic records of the region. Homogenization approaches are supposed to correct also this kind of biases by comparing temperatures recorded in urban areas against those of their surrounding and still rural ones.

However, homogenization approaches have limits. For example, when large regions undergo a significant and diffused urbanization process it is objectively difficult to clean the records of any urbanization bias. In these densely connected urban networks, the leftover rural areas are themselves surrounded by growing UHIs. Thus, the warming produced by the urban regions can spread over the rural ones as well. Moreover, if the UHIs' network is dense, homogenization processes can corrupt the temperature records of the less urbanized stations by transferring into them a fraction of the warming bias of their urban neighbors (de Gaetano, 2006; Pielke Sr. et al., 2007a, 2007b). In these cases, homogenization processes may be inefficient, and the resulting climatic records could artificially show recent periods warmer and early periods cooler.

Several mechanisms regulate the UHI phenomenon and may vary from region to region, and urban area to urban area. For example, in some desertic climates, urbanization can lead to urban cooling, while in polar latitudes the role of direct building heating can be more important. The physical property used in this work is that UHI effects vary according to season and the time of day.

In fact, UHI is generally greatest during calm, warm weather, and is most pronounced at night. This dynamic is better explained in Fig. 1 showing the evolution of the boundary layers above an urban area and its surrounding countryside both during day and night (Oke, 1987; Stull, 1988; Kershaw, 2017). During the daytime, UHI is more localized and, therefore, its area of influence is smaller because the surface, including the urban areas, gets warm by sunlight. The warm surface activates a convective instability resulting in a vertical flux of warm air parcels. As a result, the surface is prevented by vertical convection processes to warm excessively by trapping heat and pollutants. In other words, during the daytime, the capping inversion layer is usually relatively high from the surface and the warm air produced by the city can more likely diffuse vertically. Consequently, the cities' warm air has fewer chances to warm surrounding areas. On the contrary, during

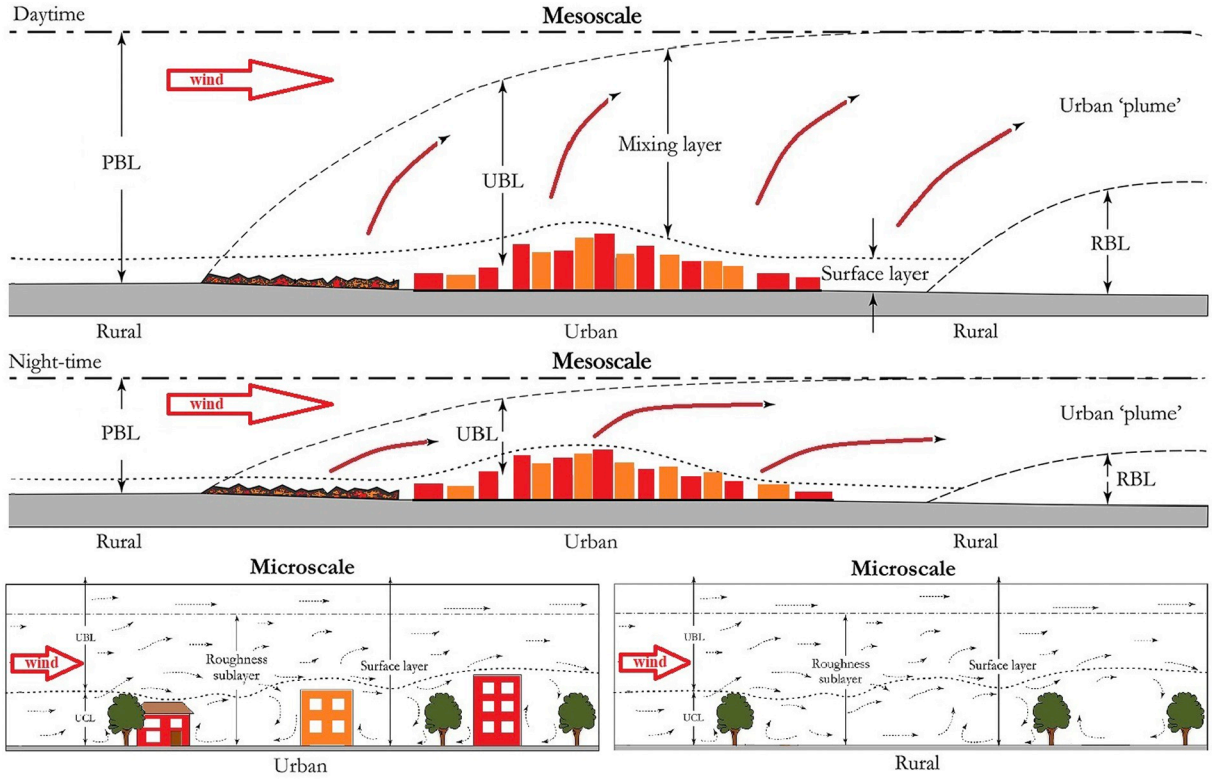

Fig. 1. Boundary layer structure over a city and its surrounding area. Top, daytime boundary layers; middle, nocturnal boundary layers; bottom, microscale structures showing how the wind extracts heat from an urban area and may transport it away from it toward the rural areas. Planetary boundary layer (PBL); Urban boundary layer (UBL); Urban canopy layer (UCL). (Adapted from Kershaw, 2017).

nighttime, the UHI area of influence enlarges because the surface cools fast forming a low capping inversion layer that prevents an equally strong vertical air convection flux. Consequently, more heat is trapped in the contracted boundary layer near the surface. Nocturnal surface winds, even the weak ones, can then more easily spread this warm air into the surrounding rural regions and contrast their fast cooling due to their higher evaporation, radiation, and convection. Moreover, urban landscapes warm slowly during the daytime because of buildings shading and the high heat capacity of their materials. However, once warmed, they also slowly lose the accumulated heat to the atmosphere and remain warmer than the surrounding environment during nighttime. For the same reason, also heat radiated directly from the warm cities toward the surrounding rural areas warm them more during nighttime than daytime. For the above reasons, one should expect that rural or suburban areas are more exposed to the heat produced by the surrounding UHIs during nights.

These mechanisms appear confirmed for some Chinese cities like Beijing where the increase in surface air temperature due to urban surface expansion was not symmetrical, being smaller in the daytime and larger at night over the past 37 years (Zhao and Wu, 2019). It has been also noted that absorbing aerosol could induce a day time cooling over some China regions (Cai et al., 2016), yet this phenomenon, while affecting the local Tmean trend estimates, appears different from the UHI effect that should still induce a Tmin warming larger than the Tmax one.

Similar physical mechanisms would predict that over China during summertime the warmer surface activates a convective instability resulting in the vertical flux of warm air parcels limiting a heat diffusion from the UHIs toward the surrounding rural areas. On the contrary, during wintertime, the boundary layer above urban and rural areas contracts and the heat produced by the urban area could more easily spread toward the surrounding areas and warm them. Note that during the six coldest months (from November–April) of the year anticyclonic conditions, centered upon Siberia, usually form also over China. High-pressure conditions contract the boundary layers and activate the weak winter monsoons flowing from land to ocean (Hartmann, 2016). On the contrary, during the six warmer months (from May to October) of the year, cyclonic conditions usually develop above China. Low-pressure conditions vertically expand the boundary layers and activate the strong summer monsoons flowing from ocean to land (Hartmann, 2016).

Similarly, winds coming from the open ocean are UHI free and can mitigate urbanization biases also above land nearby the coasts. Diurnal sea breeze would dilute UHI whereas nocturnal land breeze will move the warm city air toward the ocean away from the inland rural meteorological stations. Thus, urbanization bias could warm continental region more than the coastal ones. Therefore, south-east China could be less affected despite the presence of large cities because the summer monsoons come mostly from that direction.

In conclusion, if the temperature records still present an uncorrected urbanization bias after being processed with homogenization algorithms, we should expect that the nightly temperature records present warming trends larger than the daily ones. An urbanization bias should be more pronounced during the coldest months of the year than during the warmer ones. Finally, we should also expect that urbanization bias is more pronounced in the continental regions than in the coastal ones. Finally, south-east China may be less affected by such problems.

Historical weather stations have often used Max/Min thermometers that record the daily minimum (on average around 6:00 am just before sunrise) and maximum (on average 1–2 h after noon) temperature values. These values are indicative of the nighttime and daytime temperatures and are typically labeled as Tmin and Tmax. The daily, monthly and annual temperature means, which are typically used in climatology, are usually calculated by averaging Tmin and Tmax. However, averaging conceals the important physical information contained in the differences observed between Tmax and Tmin values.

Most of the Chinese stations have adopted a fixed observing time regime after 1950. Therefore, controversies still exist over time of observation bias (TOB) (e.g., Karl et al., 1986; Tang and Ren, 2005; Tang et al., 2010). In any case, in the following, we will use the CRU Tmin and Tmax records assuming that they are sufficiently reliable since the 1940s (Jones, 2016).

In the following, we test the above conjectures by studying how Tmin and Tmax records have diverged from each other in China since the 1940s. The expected theoretical behaviors are assumed to be those produced by the available CMIP5 GCMs' ensemble mean simulations (Bindoff et al., 2013). A comparison of the results against urbanization development maps of China would eventually confirm the existence of an urbanization bias behind our temperature results. This research has, therefore, the aim of identifying the Chinese regions where urbanization biases could still be relevant and, also, to provide an approximate local magnitude of their significance.

1.2. The current and early 20th century warm periods in China

A still highly controversial issue regards how much the current post-2000 warm period has been warmer relative to the earlier one occurred in the 1940s. Li et al. (2017), Cao et al. (2013) and Wang et al. (2014) claimed that the current warm period is the hottest on record by a substantial amount. Other studies, instead, suggested that the current warm period has been only moderately warmer than the previous one (Wang et al., 2001, 2004; Tang and Ren, 2005; Tang et al., 2010; Ren et al., 2012, 2017; Ding et al., 2014). Finally, Soon et al. (2015) found that the early 20th-century warm period could have been the hottest on record for China. Herein we observe that these studies have used Tmean records, mostly at the annual scale. Tang and Ren (2005), Tang et al. (2010) and Li et al. (2017) specifically avoided using Tmean records because they were concerned about the pre-1950 changes in observing times. Instead, they calculated Tmean from the average of Tmax and Tmin. However, our point is that Tmax and Tmin must be studied independently. Moreover, in the presence of urbanization bias, the results could depend on the location. All these facts might have contributed to the above uncertainty. Our analysis will try to clarify the situation.

In any case, using worldwide climatic records, several studies have determined that two warm periods around the 1940s and the 2000s have been likely induced by a 60-year natural oscillation. It was characterized by a 1919–1940 warming phase, a 1940–1970 cooling phase, 1970–2000 warming phase and a nearly stationary temperature level since 2000; during the 20th century, this 60-year oscillation has been superimposed to a longer scale warming trend (e.g.: Gervais, 2016; Scafetta, 2013a, 2013b, Scafetta, 2014a, 2014b; Wyatt and Curry, 2014; and many others). This 60-year cycle is found also in solar and astronomical records (e.g.: Scafetta, 2012; Scafetta et al., 2016). The warming secular trend might be due to anthropogenic forcing superimposed to longer natural climatic cycles (e.g.: Scafetta, 2013a, 2013b; Scafetta et al., 2016). For example, a millennial natural oscillation has been in its warm phase since the Little Ice Age of the 17th century and could have contributed to the secular warming observed since 1900 (e.g.: Hoyt and Schatten, 1993; Kerr, 2001; Kirkby, 2007; Christiansen and Ljungqvist, 2012; Scafetta, 2014b). We will use the results of our analysis to estimate the likely warming that occurred from the 1940s to the 2000s over China.

Evaluating how warmer the post-2000 warm period could have been relative to the 1940s one is also useful to quantify the anthropogenic warming due to greenhouse gas (GHG) emissions because most of such emission occurred after 1950 (cf. Bindoff et al., 2013).

1.3. Methodological approach

Our approach does not aim to show that different climatic records collected independently from each other present different results. Nor we separate urban from rural temperature records since such a operation may also be hypothetical and arbitrary (Stewart and Oke, 2012). Other approaches used to separate urban and rural regions using for example night-light metadata (Peterson, 2003) may be unsatisfactory too since heat may move from UHIs to suburban or rural regions because of the different wind dynamics during day and night and through infrared radiation. Adopting such methodological approaches, which attempt to a priori separate the UHI affected and not affected regions, may just not solve any controversy.

This study proposes a workaround methodology. We aim to show that the same set of temperature records in their three forms of Tmax, and Tmin (note that each meteorological station measures daily Tmax and Tmin values using the same instrument), and their derived Tmean show different secular trends because of their different physical meanings. We then correlate these differences with urbanization development patterns to determine the likeliness that the observed divergence may be due to a UHI bias. Finally, we will explain the encountered spatial differences also by relating them with the characteristics of the local climates and will complete our study by adding a seasonal analysis.

We note that Parker (2006) too similarly avoided sorting stations according to “urban” or “rural” but sorted data according to “windy” or “calm” days and claimed that large-scale warming was not affected by an urbanization bias because windy days were just slightly cooler than the calm ones, but the trends were unaffected. Parker's approach is, however, different from the one herein proposed because we do not make such a sorting either because even weak winds would be able to move warm air from urban to suburban or nearby rural areas, and heating by radiation would work both in windy and calm days. As explained, through many physical mechanisms, UHI is supposed to influence larger areas during nighttime because the atmospheric boundary layer contracts and the warm urban bubble spreads around.

2. Data

We use the Climate Research Unit (CRU) (University of East Anglia) global land surface temperature datasets (CRU TS4.01) (update of Harris et al., 2014; Jones et al., 2012) (https://crudata.uea.ac.uk/cru/data/hrg/cru_ts_4.01/). This record covers the period 1901–2016 with a spatial resolution of $0.5^{\circ} \times 0.5^{\circ}$. The maximum, mean and minimum near-surface temperature datasets are herein labeled as Tmax, Tmean and Tmin, respectively. The same temperature records over China alone are available at Climate Change Atlas at KNMI Climate Explorer (https://climexp.knmi.nl/plot_atlas_form.py). According to the Global Historical Climatology Network (GHCN: https://www.ncdc.noaa.gov/ghcn-daily-description) most of China has been covered by meteorological stations at least since the middle of the 20th century (cf.: Soon et al., 2018; Wang and Chen, 2016). In any case, the CRU Tmax and Tmin records cover the entire region at least since 1940. Fig. 2 shows the distribution of the GHCN weather stations over China with Tmax and Tmin records.

We also use the Coupled Model Intercomparison Project Phase 5 (CMIP5: https://cmip.llnl.gov/cmip5/) (full set) GCM ensemble mean simulations of maximum, mean and minimum near-surface temperature over China available at Climate Change Atlas at KNMI Climate Explorer (https://climexp.knmi.nl/plot_atlas_form.py). The chosen computer simulations adopt the full set of historical radiative forcings from 1860 to 2005 and the representative concentration pathway (RCP) 8.5 scenario forcings from 2006 to 2100. From 2006 to 2015 the simulations available for alternative RCP (2.6, 4.5, 6.0, 8.5) are statistically equivalent and we explicitly use the RCP 8.5 ones (Bindoff et al., 2013).

Our hypotheses are tested against the population distribution and urbanization development in China since 1950 from the National Bureau of Statistics of China (http://data.stats.gov.cn) (cf. Wang and Chen, 2016). We also use data from the Population Division of the Department of Economic and Social Affairs of the United Nations (https://population.un.org/wup/). Since 1988 this organization has

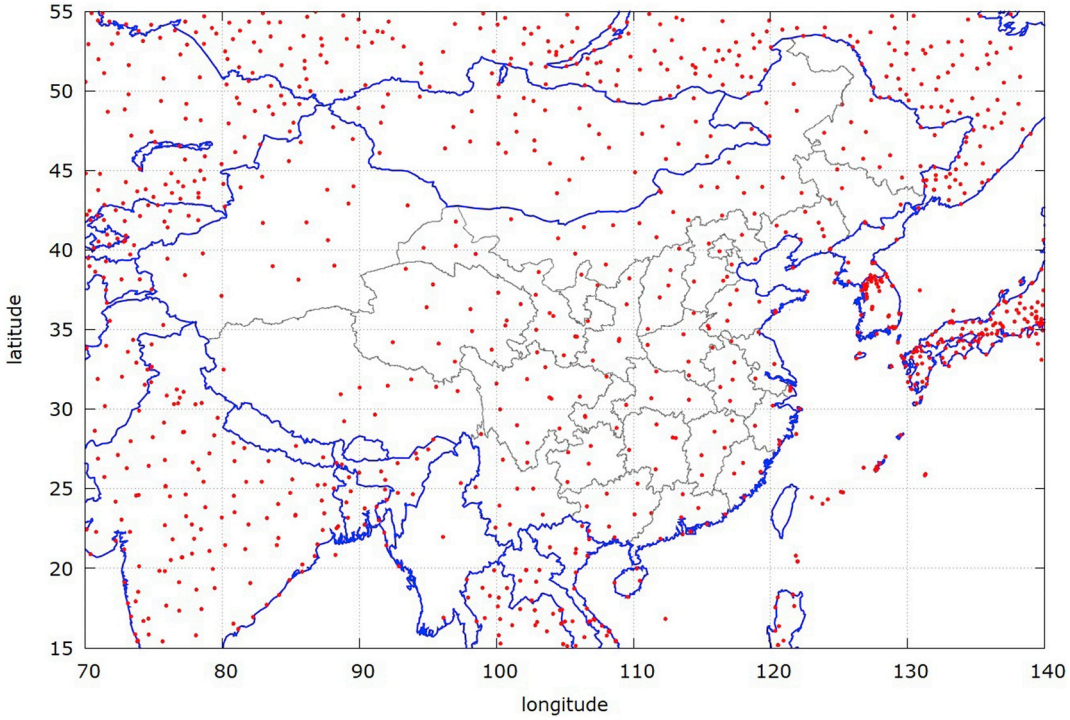

Fig. 2. Distribution of meteorological stations of the Global Historical Climatology Network where Tmax and Tmin temperature records are available.

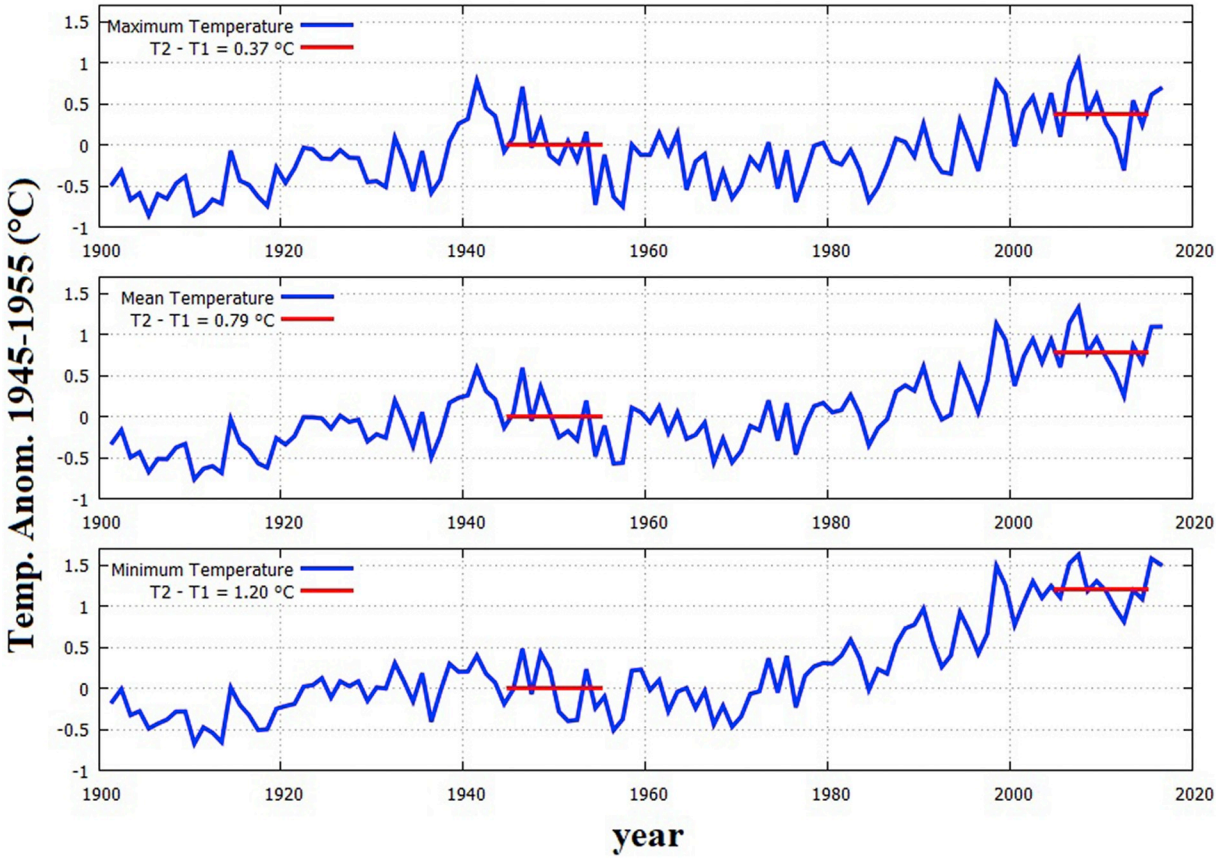

Fig. 3. CRU TS4.0 Tmax, Tmean and Tmin over China obtained from KNMI Climate Explorer. The red segments indicate the mean temperature values, T_1 and T_2, in the 1945–1954 and 2005–2014 decades. (For interpretation of the references to colour in this figure legend, the reader is referred to the web version of this article.)

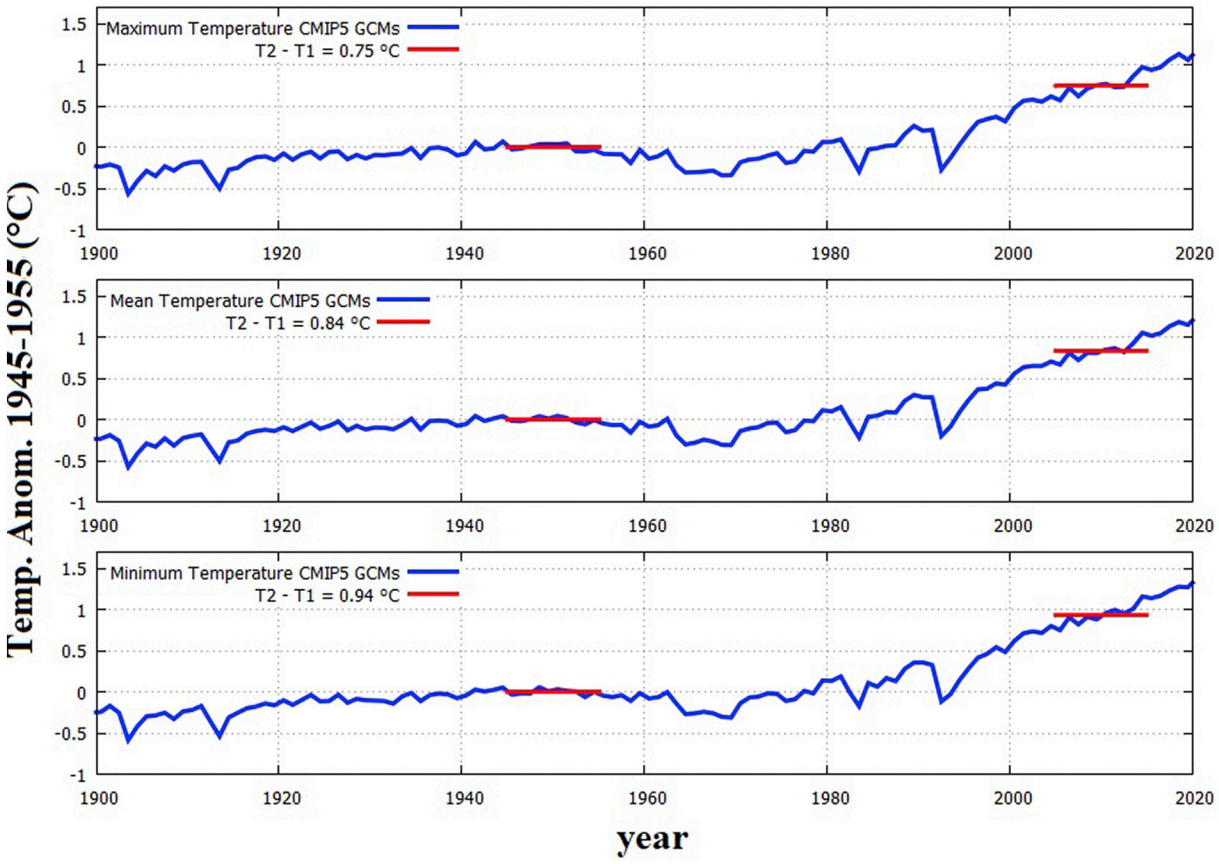

Fig. 4. CMIP5 GCM Tmax, Tmean and Tmin near-surface annual ensemble average temperature records over China obtained from KNMI Climate Explorer. The red segments indicate the mean values T_1 and T_2 in the 1945–1954 and 2005–2014 decades. (For interpretation of the references to colour in this figure legend, the reader is referred to the web version of this article.)

been issuing revised estimates and projections of the urban and rural populations of all countries in the world and their major urban agglomerations, including China.

3. Analysis of the Tmax and Tmin network in China from 1945–1954 to 2005–2014

Fig. 3 shows the CRU TS4 Tmax, Tmean and Tmin near-surface annual average temperature records over China obtained from KNMI Climate Explorer. The records are anomalies relative to the decade 1945–1954. The figure highlights the warming of the three records between the decades 1945–1954 and 2005–2014.

This 60-year period has been chosen for four reasons: 1) the Chinese temperature network before this period is less homogeneous (cf. Soon et al., 2018); 2) the urbanization development of China occurred mostly after the 1945, that is after World War II; 3) to reduce possible statistical artifacts due to a plausible 60-year oscillation that is observed in climatic records all over the world (e.g.: Gervais, 2016; Scafetta, 2013a, 2014a; Wyatt and Curry, 2014); 4) to avoid possible statistical artifacts due to the strong 2015–2016 El-Nino effect (e.g.: Scafetta et al., 2017a, 2017b). The temperature records of China depicted in Fig. 3 show a similar 60-year warming-cooling oscillating pattern superimposed to a secular warming trend (cf: Soon et al., 2015, 2018).

From 1945–1954 to 2005–2014 the mean land surface temperature in China warmed by about 0.79 °C. However, during the same period, Tmax increased by 0.37 °C while Tmin increased by 1.20 °C. Thus, on average, over China, Tmin warmed about 0.83 °C more than Tmax. By comparison, Fig. 4 shows the ensemble mean annual Tmax, Tmean and Tmin near-surface temperature records produced by the CMIP5 ensemble average simulations. The records are again anomalies relative to the 1945–1954 decade. The simulations do not show any 60-year oscillation with its characteristic 1940s warm period observed in the data (cf.: Scafetta, 2013a). They only show a warming trend since 1900, which is momentarily interrupted for a few years by sudden cooling spikes due to major volcano eruptions. These include Santa Maria (1902), Mt. Agung (1962), El Chichon (1982) and Mt. Pinatubo (1991). Similar patterns are seen in the CMIP5 simulation globally (cf.: Bindoff et al., 2013). According to these computer climate simulations, from 1945–1954 to 2005–2014 the mean land surface temperature in China had to warm by 0.84 °C. This warming is slightly higher than the observed one (0.79 °C). However, during the same period, the synthetic Tmax increased by 0.75 °C while the synthetic Tmin increased by 0.94 °C. Thus, according to the CMIP5 climatic simulations in China, Tmin had to warm only about 0.19 °C more than Tmax.

Table 1 summarizes the above results. Within the statistical error of measure, the observed and simulated mean temperature increases from 1945–1954 and 2005–2014 are compatible: $\Delta T_{Mean} = 0.79 \pm 0.10$ °C (observations) versus $\Delta T_{Mean} = 0.84 \pm 0.04$ (CMIP5 simulations). However, the observed and simulated Tmax and Tmin increase from 1945–1954 and 2005–2014 are not compatible. Tmax warmed significantly less than what the models have predicted: $\Delta T_{Max} = 0.37 \pm 0.12$ °C (observations) versus $\Delta T_{Max} = 0.75 \pm 0.04$ °C (CMIP5 simulations). Conversely, Tmin warmed significantly more than what the climate models predict: $\Delta T_{Min} = 1.20 \pm 0.08$ °C (observations) versus $\Delta T_{Min} = 0.94 \pm 0.04$ °C (CMIP5 simulations). Thus, from 1945–1954 to 2005–2014, over China the CMIP5 GCM simulations predict a Tmin increase that had to be $\Delta T_{Min} - \Delta T_{Max} = 0.19 \pm 0.06$ °C warmer than the Tmax one while the CRU records show a Tmin increase that is $\Delta T_{Min} - \Delta T_{Max} = 0.83 \pm 0.15$ °C warmer than the Tmax one. Therefore, the observed divergence between observations and GCM simulations is

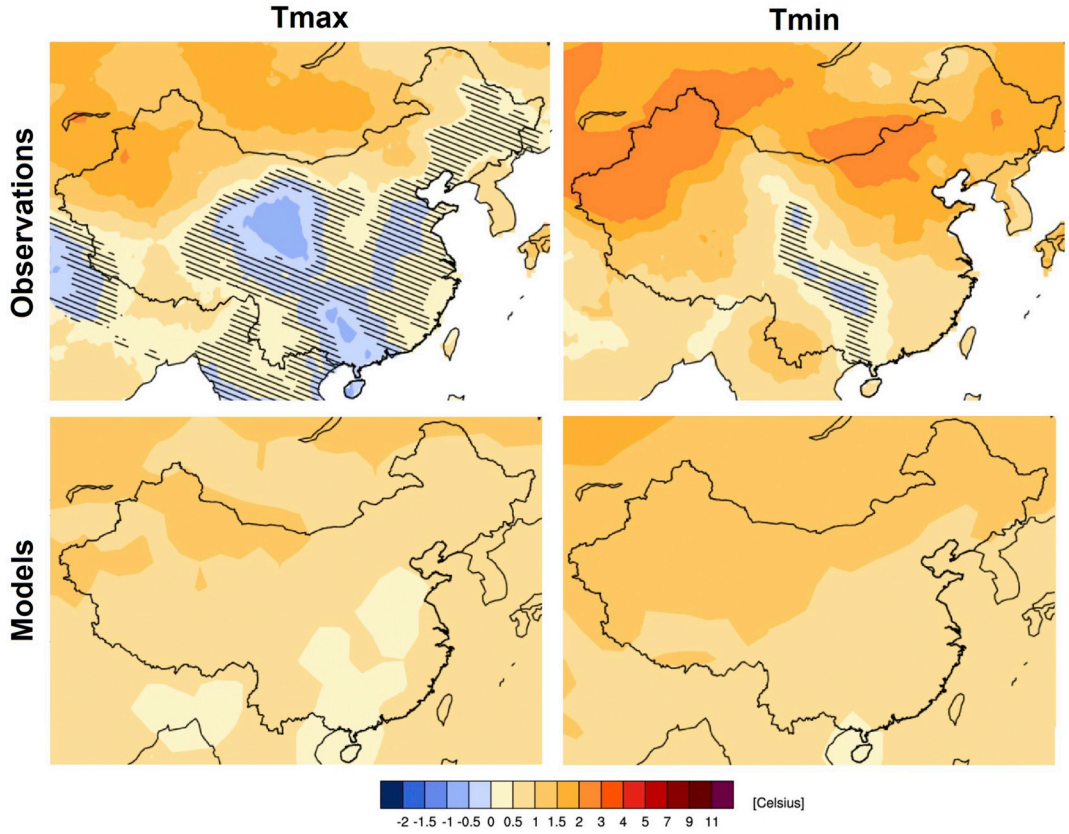

Fig. 5. (Left) Tmax and (Right) Tmin. The maps show the 2005–2014 mean value minus 1945–1954 mean value. (top) Temperature observations (CRU TS4) and (bottom) full CMIP5 GCM mean ensemble simulation. The maps are centered over China. The hatching represents areas where the signal is smaller than one standard deviation of natural variability (e.g. the value is nearly zero).

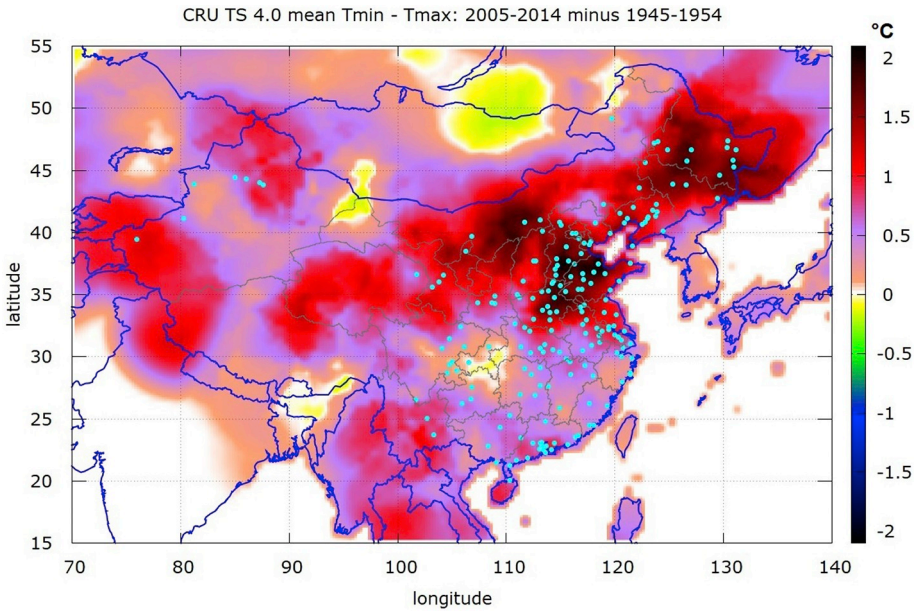

Fig. 6. Map of the divergence ($\Delta T_{Min} - \Delta T_{Max}$) between the warmings registered by the minimum and maximum temperature records (CRU TS4) between 1945 and 1954 and 2005–2014. The cyan dots indicate the 200 most populated cities in China according to the Free World City Database. (White regions over India and the ocean indicate missing data). (For interpretation of the references to colour in this figure legend, the reader is referred to the web version of this article.)

statistically significant.

Fig. 5 shows maps of the temperature variation ΔT_{Max} and ΔT_{Min} between the 1945–1954 and 2005–2014 periods using both the CRU records and the CMIP5 ensemble mean simulations. The figure shows that ΔT_{Max} increased moderately or even decreased in large areas of China. ΔT_{Min} increased significantly more in most of China. By contrast, the CMIP5 simulations show a significantly homogeneous pattern with both ΔT_{Max} and ΔT_{Min} increasing over China with ΔT_{Min} just slightly warmer than ΔT_{Max}. This figure again suggests a significant divergence between the observed and synthetic climatic records.

A quantitative analysis is now presented using the spatial high-resolution CRU TS4.01 0.5°x0.5° gridded record over China. For each 0.5°x0.5° cell we evaluate the mean values for the 1945–1954 and 2005–2014 decades, for both the minimum and maximum temperature records. Their difference, $\Delta T_{Min} - \Delta T_{Max}$, is plotted in Fig. 6. It also shows, as cyan dots, the position of the 200 most populated cities in

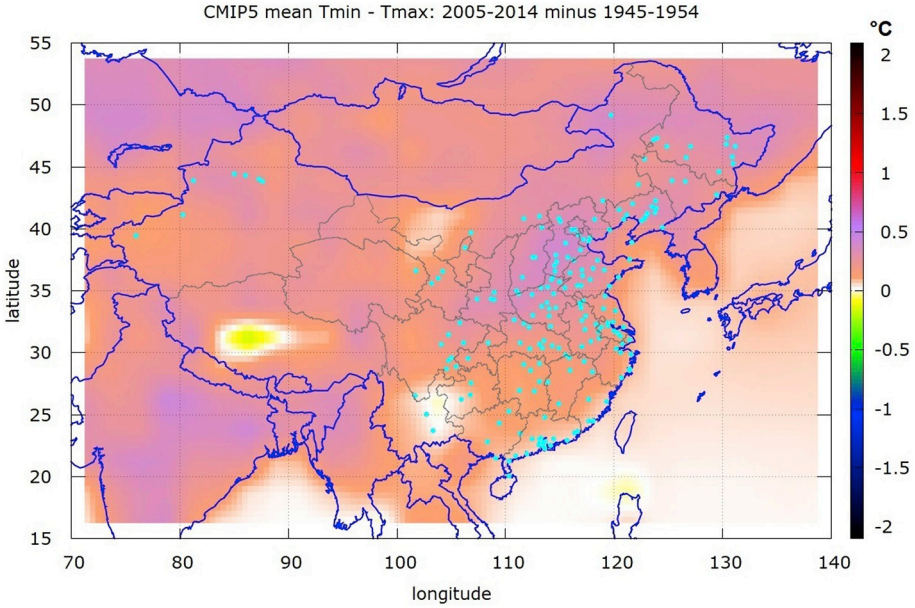

Fig. 7. Like Fig. 6 using the CMIP5 GCM predictions.

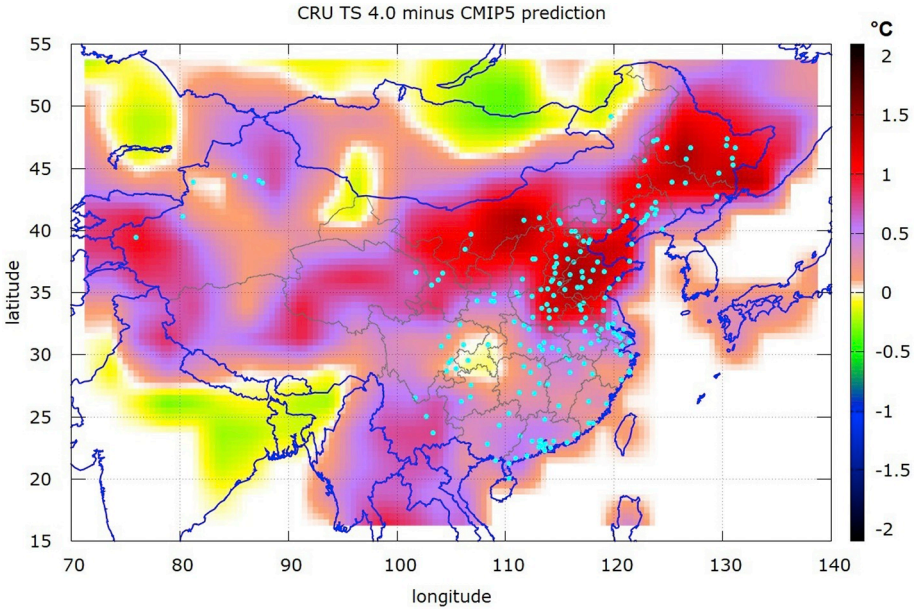

Fig. 8. Fig. 6 minus Fig. 7.

China according to the Free World City Database (worldcitiespop.txt, 2012). This figure demonstrates that over China the divergence ($\Delta T_{Min} - \Delta T_{Max}$) between the minimum and maximum temperature records from 1945–1954 and 2005–2014 varies greatly from nearly 0 °C to 2 °C.

Evident regional patterns are noted. The region with the highest divergence (red-black colour) is North-East China [112°–120°E:32°–40°N]. It mostly includes the Chinese provinces of Beijing, Tianjin, Jiangsu, Shandong, Henan, Anhui, and Hebei. By contrast, Fig. 7 repeats the same analysis using the CMIP5 GCM synthetic records and shows that the same variable is nearly homogeneous over China: the value varies approximately around 0.0–0.4 °C. Fig. 8 finally shows the difference between Fig. 6 and Fig. 7, and demonstrates that for vast regions of China, $\Delta T_{Min} - \Delta T_{Max}$ is significantly larger than what the models predict: the divergence reaches about 1.5 °C in the highly densely populated North-East China [112°–120°E:32°–40°N].

This result is further stressed in Fig. 9 that compares the observed and synthetic Tmax and Tmin over the selected [112°–120°E:32°–40°N] region. From 1945–1955 to 2005–2015, Tmax remained nearly the same ($\Delta T_{Max} = 0.05 \pm 0.13$ °C) while Tmin increased by about 1.5 °C ($\Delta T_{Min} = 1.52 \pm 0.11$ °C). Thus, $\Delta T_{Min} - \Delta T_{Max} = 1.47 \pm 0.16$ °C. By contrast, the CMIP5 simulations predict a Tmax increase of $\Delta T_{Max} = 0.47 \pm 0.05$ °C and a Tmin increase of $\Delta T_{Min} = 0.76 \pm 0.04$ °C. Thus, $\Delta T_{Min} - \Delta T_{Max} = 0.29 \pm 0.06$ °C. The observed divergence between Tmin and Tmax in the CRU ST4 observations is about 5 times larger than that found in the CMIP5 synthetic records, so it is statistically significant. If the decades are changed as 1955–1964 and 2005–2014, and as 1965–1974 and 2005–2014, when the temperature network over China was likely more functional and standardized, ΔT_{Min} would still be about 1 °C warmer than ΔT_{Max} against mean 0.3 °C predicted by the models. See the Appendix.

Fig. 10 shows the statistical cumulative distribution of the $\Delta T_{Min} - \Delta T_{Max}$ values depicted in Fig. 6 over China alone. Each value was

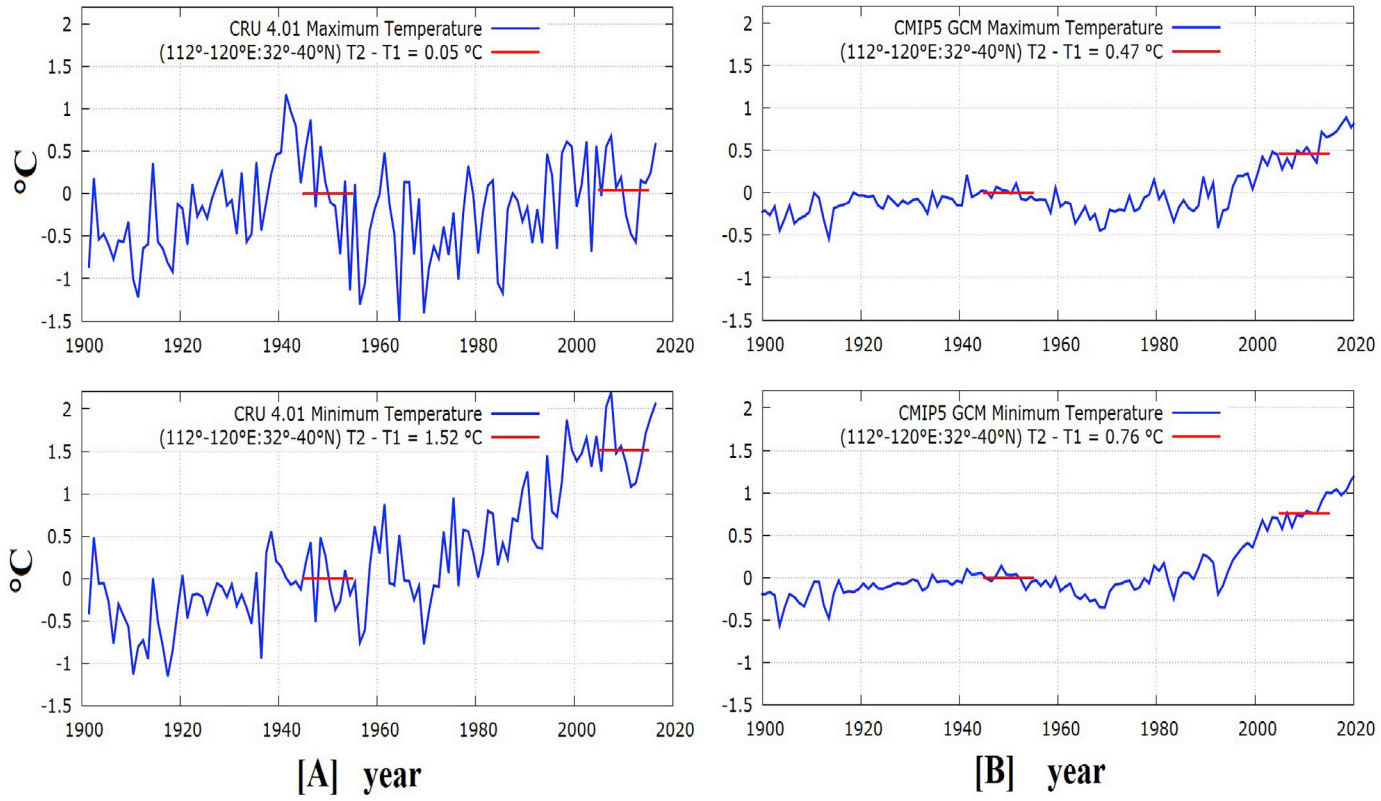

Fig. 9. [A] CRU TS4 Tmax and Tmin near-surface annual average temperature records. [B] CMIP5 maximum, mean and minimum near-surface annual ensemble average temperature records. Region [112°–120°E:32°–40°N]. The red segments indicate the mean values, T_1 and T_2, in the 1945–1954 and 2005–2014 decades. (For interpretation of the references to colour in this figure legend, the reader is referred to the web version of this article.)

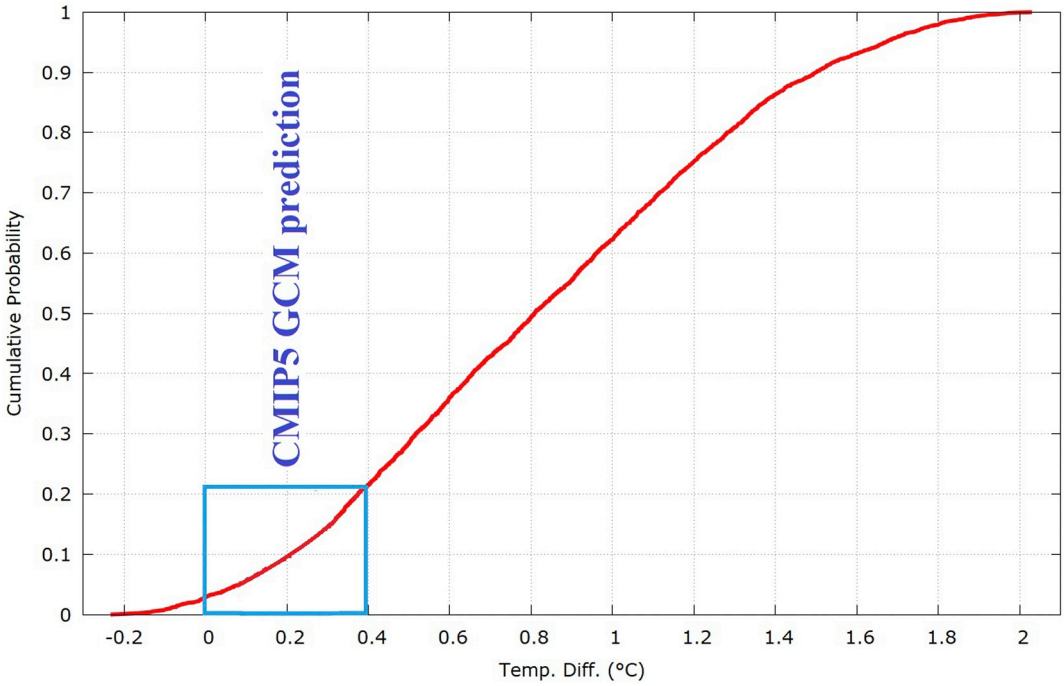

Fig. 10. The fraction of the surface area of China characterized by $\Delta T_{Min} - \Delta T_{Max} <$ Temp. Diff.: cf. Fig. 6. The blue box represents the approximate variability predicted by the CMIP5 GCM models: cf. Fig. 7. (For interpretation of the references to colour in this figure legend, the reader is referred to the web version of this article.)

weighted with the cosine of the latitude to make the measure proportional to the correspondent surface area. The red curve indicates the fraction of the surface area of China characterized by a $\Delta T_{Min} - \Delta T_{Max}$ value lower than the given value of the abscissa. The blue box covers the interval of 0.0–0.4 °C that is the approximate variability predicted by the CMIP5 GCM models. Fig. 10 indicates that about 20% of the

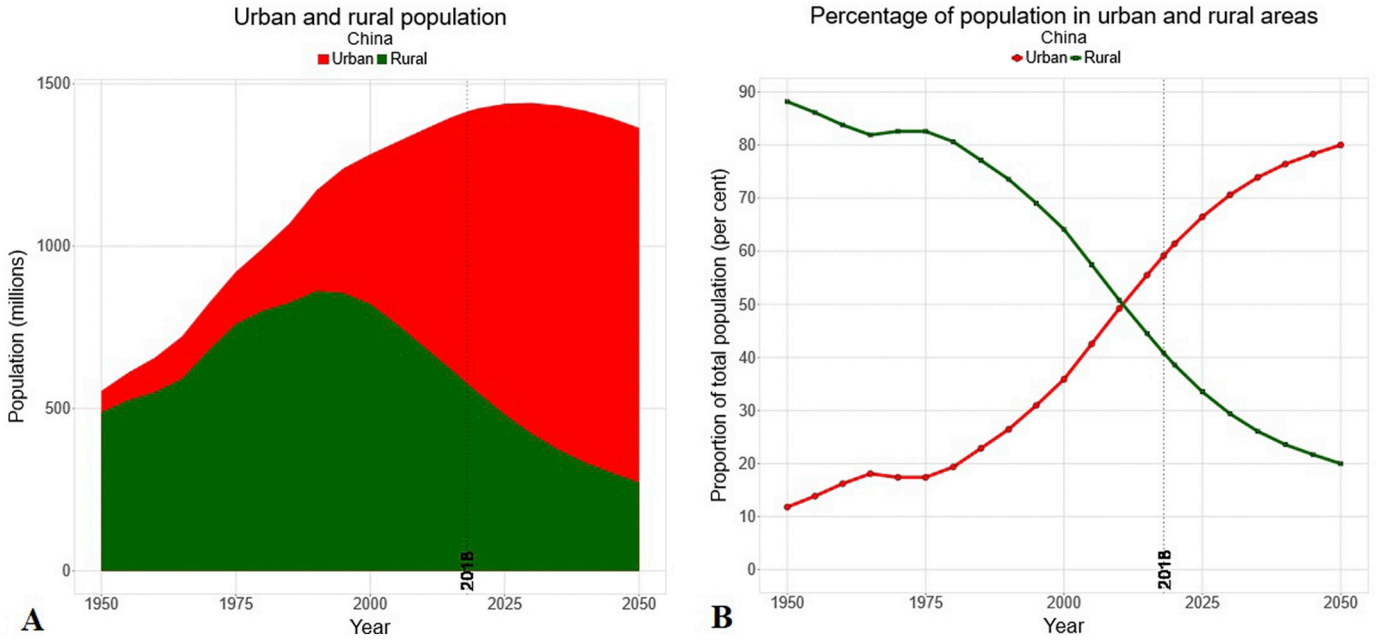

Fig. 11. [A] Evolution of the urban and rural populations in China: measured from 1950 to 2018; expected from 2018 to 2050. [B] The same as a percentage of the total population of China.

Table 2
The annual population of 426 urban agglomerations in China (including Macao and Hong Kong) with 300 K or more people in 2018.

Population	1950	1960	1970	1980	1990	2000	2010	2020
1 K–50 K	266	242	197	111	20	0	0	0
50 K–100 K	52	43	60	107	80	0	0	0
100 K–300 K	75	93	109	120	188	162	67	0
300 K–500 K	14	22	20	40	66	115	148	120
500 K–1 M	10	13	25	29	37	84	124	171
1 M–5 M	9	12	14	17	32	57	71	114
5 M–10 M	0	1	1	2	3	6	10	15
10 M–30 M	0	0	0	0	0	2	6	6

The data for 2020 are model expectations. (Source: United Nations, World Urbanization Prospects 2018).

surface of China presents the same $\Delta T_{Min} - \Delta T_{Max}$ values predicted by the climate models, as also Fig. 8 would suggest. Nearly 40% of the surface of China presents $\Delta T_{Min} - \Delta T_{Max}$ values between 0.4 and 1.0 °C; nearly 30% presents $\Delta T_{Min} - \Delta T_{Max}$ values between 1.0 and 1.5 °C; and 10% presents $\Delta T_{Min} - \Delta T_{Max}$ values between 1.5 and 2.1 °C. Again, the result demonstrates that there is a significant divergence between the CRU TS4.01 climatic records and the CMIP5 GCM synthetic ones.

4. Urbanization development in China since 1950

Urbanization significantly transforms the landscapes from rural to urban and could be more pronounced in some regions than in others. Thus, the issue is to determine how in China the urbanization has developed since about 1950 and whether some regions have experienced a more significant and diffused urbanization than others.

To test the above hypothesis, we now briefly study the population distribution and urbanization development in China from 1950 to 2010 (cf. Wang and Chen, 2016). Data are also available from the Population Division of the Department of Economic and Social Affairs of the United Nations (https://population.un.org/wup/) and the National Bureau of Statistics of China (http://data.stats.gov.cn).

According to the United Nations, in China the annual urban population increased from 65 million in 1950 to 775 million in 2015: this is a 12 times increase in just 65 years. On the contrary, the annual rural population increased from 489 million in 1950 to 622 million in 2015: a 27% increase. While in 1950 only 12% of the entire population of China lived in the urban areas, in 2015 55% of China 1.4 billion people lived in urban agglomerations. By contrast, most regions of the world experienced a significant minor transformation. For example, in Europe the urban population increased from 284 million (1950) to 547 million (2015), that is, it just nearly doubled, while the rural population decreased from 265 million (1950) to 194 million (2015).

Fig. 11 shows the urban and rural population change in China from 1950 to 2018 and its possible development from 2018 to 2050 according to the United Nations. China large urbanization since 1950 is further demonstrated in Table 2 that shows how the population distribution of 426 urban agglomerations in China (including Macao and Hong Kong) with 300 K or more people in 2018 evolved since 1950. Of these 426 urban agglomerations, 393 had a population of fewer than 300 K units in 1950. Just 9 urban agglomerations had a population above 1 million in 1950 whereas, in 2010, 87 urban agglomerations had above 1 million people. Of these 87 urban agglomerations, 4 had less than 5000 people in 1950: for example, Shenzhen, near Hong Kong, increased its population from 3000 people in 1950 to more than 10 million in 2010. Table 3 reports how the population of the provinces of China evolved according to the censuses in 1953, 1964, 1982, 1990, 2000, and 2010.

Fig. 12 shows several population-density maps over China. Fig. 12A is a typical geographic population density map that shows well how east and west China are very differently populated. Fig. 12B shows a map from the United Nations World City Population indicating the urban agglomeration population growth from 1950 to 2035. The circled areas are proportional to the city populations in 1950 (the darkest blue), 1990 (darker blue), 2015 (blue), and the expected population in 2035 (very light blue). Fig. 12C and D compare the population of each of the provinces of China in 1954 and 2010 (cf. Wang and Chen, 2016).

A visual comparison between Figs. 6, 8 and 12 clearly indicates that the regions marked in Figs. 6 and 8 by red-black colour (that is the ones with the highest divergence between ΔT_{Min} and ΔT_{Max}) fall within the most densely populated provinces in east-China with more than 400 people/km^2: see Table 3. This region mostly includes the provinces of Beijing, Tianjin, Jiangsu, Shandong, Henan, Anhui, and Hebei (7 out of the 10 most densely populated provinces of China: Table 3). The areas

Table 3
The population of China (in million) by province according to 6 censuses between 1953 and 2010.

Province	1953	1964	1982	1990	2000	2010	Ratio 2010/1953	Surface (km^2)	Density (2010) (people/km^2)
Shanghai	6.2	10.8	11.9	13.3	16.7	23.0	3.7	6341	3630
Beijing	3.8	8.6	9.2	11.8	13.8	19.6	5.2	16,409	1195
Tianjin	2.7	6.9[a]	7.8	8.8	10.0	12.9	4.8	11,917	1086
Jiangsu	41.3	44.5	60.5	67.1	74.4	77.7	1.9	102,600	757
Shandong	48.9	55.5	74.4	84.4	90.8	95.8	2.0	157,100	610
Guangdong	32.1[b]	39.5[b]	54.7[b]	58.0[b]	86.4	104.3	3.2	179,700	580
Henan	44.2	50.3	74.4	85.5	92.6	94.0	2.1	167,000	563
Zhejiang	22.9	28.3	38.9	41.4	46.8	54.4	2.4	101,800	535
Anhui	30.3	31.2	49.7	56.2	59.9	59.5	2.0	140,100	425
Hebei	36.0	42.8[a]	53.0	61.1	67.4	79.9	2.2	188,800	423
Chongqing	16.4[c]	17.9[c]	26.3[c]	28.3[c]	30.9	28.8	1.8	82,400	350
Hunan	33.2	37.2	54.0	60.7	64.4	65.7	2.0	211,800	310
Hubei	27.8	33.7	47.8	54.0	60.3	57.2	2.1	185,900	308
Fujian	13.1	16.8	25.9	30.1	34.7	36.9	2.8	123,900	298
Liaoning	18.5	26.9	35.7	39.5	42.4	43.7	2.4	148,400	295
Jiangxi	16.8	21.1	33.2	37.7	41.4	44.6	2.7	166,900	267
Hainan	2.7[b]	3.3[b]	4.6[b]	4.8[b]	7.9	8.7	3.2	35,354	245
Shaanxi	15.9	20.8	28.9	32.9	36.1	37.3	2.4	156,700	238
Shanxi	14.3	18.0	25.3	28.8	33.0	35.7	2.5	156,700	228
Guizhou	15.0	17.1	28.6	32.4	35.3	34.7	2.3	176,200	197
Guangxi	19.6	20.8	36.4	42.2	44.9	46.0	2.4	237,600	194
Sichuan	45.9[c]	50.0[c]	73.4[c]	78.9[c]	83.3	80.4	1.8	486,100	165
Jilin	11.3	15.7	22.6	24.7	27.3	27.5	2.4	187,400	147
Yunnan	17.5	20.5	32.6	37.0	42.9	46.0	2.6	394,100	117
Ningxia	1.5	2.1	3.9	4.7	5.6	6.3	4.2	66,400	95
Heilongjiang	11.9	20.1	32.7	35.2	39.9	38.3	3.2	454,800	84
Gansu	12.1	12.6	19.6	22.4	25.6	25.6	2.1	453,700	56
Inner Mongolia	6.1	12.3	19.3	21.5	23.8	24.7	4.1	1,183,000	21
Xinjiang	4.9	7.3	13.1	15.2	19.3	21.8	4.5	1,664,900	13
Qinghai	1.7	2.1	3.9	4.5	5.2	5.6	3.4	722,300	7.8
Tibet	1.3	1.3	1.9	2.2	2.6	3.0	2.4	1,228,400	2.4
Rehe (defunct)	5.2								
Xikang (defunct)	3.4								

The provinces ([a]), ([b]) and ([c]) were fused and the reported values are proportions based on their reported combined value and the 2010 estimate. Rehe was split among Hebei, Liaoning, Tianjin and Inner Mongolia. Xikang was split between Tibet and Sichuan. (from http://www.stats.gov.cn/tjsj/tjgb/rkpcgb/).

around the cities of Changchun (Jilin) and Haerbin (Heilongjiang) in north-east China, had a significant population increase by about 5–9 times from 1950 to 2015 and in Figs. 6 and 8 are characterized by red-dark colors. The same occurs for the areas surrounding the cities of Hohhot and Baotou (Inner Mongolia) whose urban agglomeration population increased by about 20 times from about 100 K to 2 million people from 1950 to 2015.

Another region with still a high divergence between ΔT_{Min} and ΔT_{Max} (violet-red regions) characterizes the province of Guangdong around the Hong Kong and Macao areas, on the south-east China coast (the 6th most densely populated province of China: Table 3). These regions experienced a very high urbanization development such as in the close cities of Shenzhen, Dongguan, Guangzhou, Foshan, Jiangmen and others whose urban agglomerations increased from as low as 100 K (1950) to up to about 10 million people (2015). Other regions with still a high divergence between ΔT_{Min} and ΔT_{Max} (violet-red regions) are found also in the populated area of west China (Xinjiang) and central China (Qinghai). Shanghai is the most densely populated province in China (Table 3) and in Figs. 6 and 8 also falls in this violet-red region. Here the situation could have been mitigated probably because Shanghai is on the coast and UHI effect is likely reduced by the thermal properties of the ocean and of the breezes. The same occurs for Macao and Hong Kong areas. Most of the leftover areas are still characterized by a moderately high divergence between ΔT_{Min} and ΔT_{Max} (salmon-violet regions) such as in south-east China where the large cities are more sparsely located.

The population in Chengdu and Chongqing had also grown on a large scale, by a 10 factor, comparable to many large China's cities. However, in Fig. 6 these areas [102°–110° E: 27°–31°N] are characterized only by white-light salmon colour whose $\Delta T_{Min} - \Delta T_{Max}$ is nearly 0 or about 0.3 °C. Thus, our analysis suggests that this region is mostly UHI free. Note that in this region the city network is not as dense as in the red-black areas. Fig. 12 shows also that this region is less populated than the surrounding areas. This appears in the province of Chongqing where the population seems mostly concentrated in the capital city. Thus, it is possible that in this region UHI effects have been properly cleaned out. Other explanations of the result would imply specific local weather dynamics.

Finally, coastal regions appear less affected by UHI biases relative to the continental ones despite the large population increase of some of them probably because of an oceanic thermal attenuation. For instance, Zhejiang (the 8th most densely populated province of China: Table 3) is characterized by a violet area in the north where many larger cities are located and a salmon zone in the south where the only large cities are located on the coast. There, as explained in the introduction, ocean thermal properties and breezes could have mitigated the UHI biases on the surrounding inland areas.

The web-version of the map depicted in Fig. 12B is found at http://luminocity3d.org/WorldCity/#5/31.091/108.369 and it is interactive. Population evolution graphs pop up by selecting each urban center, which is how the values discussed above were collected. For example, the insert of Fig. 12B shows the available urban agglomeration population growth for Beijing that increased from 1.7 million in 1950 to 18.4 million in 2015: that is by about 11 times in 65 years. According to Figs. 6 and 8, the same region is very dark-red colored which means that in this region Tmin increased significantly more than Tmax since 1945.

Finally, Fig. 13 shows Google-Pro satellite images of China and zooms two different areas. These photographs further explain the colour pattern shown in Figs. 6 and 8 by suggesting their urbanization origin. Fig. 13A suggests that the north-east region of China, which in Figs. 6 and 8 is characterized by a red-dark colour, is densely urbanized.

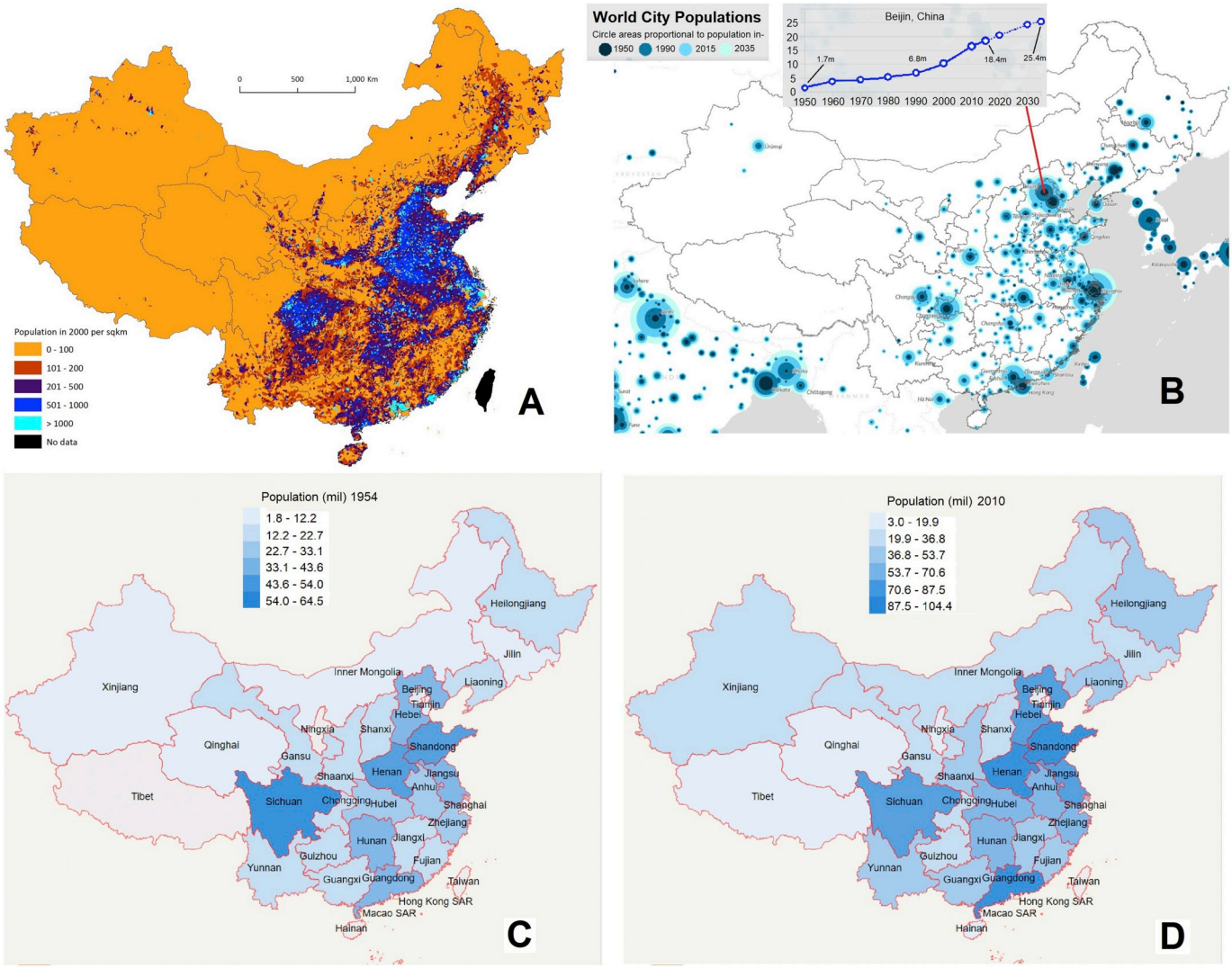

Fig. 12. [A] Population density in China (2000). Mapping prepared by Beijing City Lab (http://longy.jimdo.com). [B] Urban agglomeration population increase in China from 1950 to 1990, from 1990 to 2015 and the projected population increase between 2015 and 2035. Data from United Nations 2018. Insert Beijing's case. [C & D] Population Distribution of China in 1954 and 2010: from the National Bureau of Statistics of China (http://data.stats.gov.cn; cf. Table 3 and Wang and Chen, 2016).

The zooms depicted in Fig. 13B, C and E show that north-east China has several large cities and the land between them is uniformly filled with thousands of small towns and villages at about 2 km from each other. This dense urban network makes the entire area urbanized to some degree. The same kind of diffused urbanization is found in all red-dark zones depicted in Figs. 6 and 8. On the contrary, Fig. 13D shows the region surrounding the province of Chongqing, which in Figs. 6 and 8 is characterized by a light colour, which indicates a UHI free region. In fact, this region is very green and rural. A zoom of the photograph only shows isolated houses immersed in green areas. The inland green regions of south-east China, which appear violet in Fig. 6, are a little bit more urbanized in its main city centers. However, in this zone, highly dense and extended urban networks are only seen in the proximity of the coast and, in particular, in the province of Guangdong nearby the large cities of Guangzhou, Dongguan, Hong Kong, and Macau, whose region in Figs. 6 and 8 appears red.

Thus, there is a significant correlation between the regions of China that have experienced a significant, diffused and spatially dense urbanization since 1950 and the ones where, as Figs. 6 and 8 show, $\Delta T_{Min} - \Delta T_{Max}$ values are significantly larger than the CMIP5 GCMs predictions. This is particularly true for the region comprising Beijing, Tianjin, Jiangsu, Shandong, Henan, Anhui, and Hebei that are characterized by a dense urbanization that occupies the entire land, as Fig. 13B shows. This evidence indicates that the CRU TS 4 record contains a significant amount of uncorrected or inefficiently corrected urbanization bias. Since, as explained in the introduction, this bias is more likely to warm Tmin than Tmax, it may be possible to suggest that the real climatic temperature change over China since the half of the 20th century is better described by the Tmax record than by the Tmean record shown in Fig. 3. Even assuming that Tmin had to warm more than Tmax by about 0.2 °C, as the CMIP5 GCM simulations predict, it is quite probable that the 2005–2014 decade has been on average about 0.5 °C (or less) warmer than the 1945–1954 decade. Using Table 1, between these two periods ΔT_{Mean} should have been about $(\Delta T_{Max})_{CRU} + 0.5(\Delta T_{Min} - \Delta T_{Max})_{models} = 0.46 \pm 0.13$ °C, which is 42% less than the reported 0.79 ± 0.10 °C.

5. Seasonal behavior and the current and early 20th century warm periods

We now address the seasonality of the phenomenon and, finally, the issue raised in Soon et al. (2018) regarding how the current post-2000 warm period compares to the 1940s warm period. Table 4 compares the temperature variations observed in Tmax, Tmean and Tmin records and

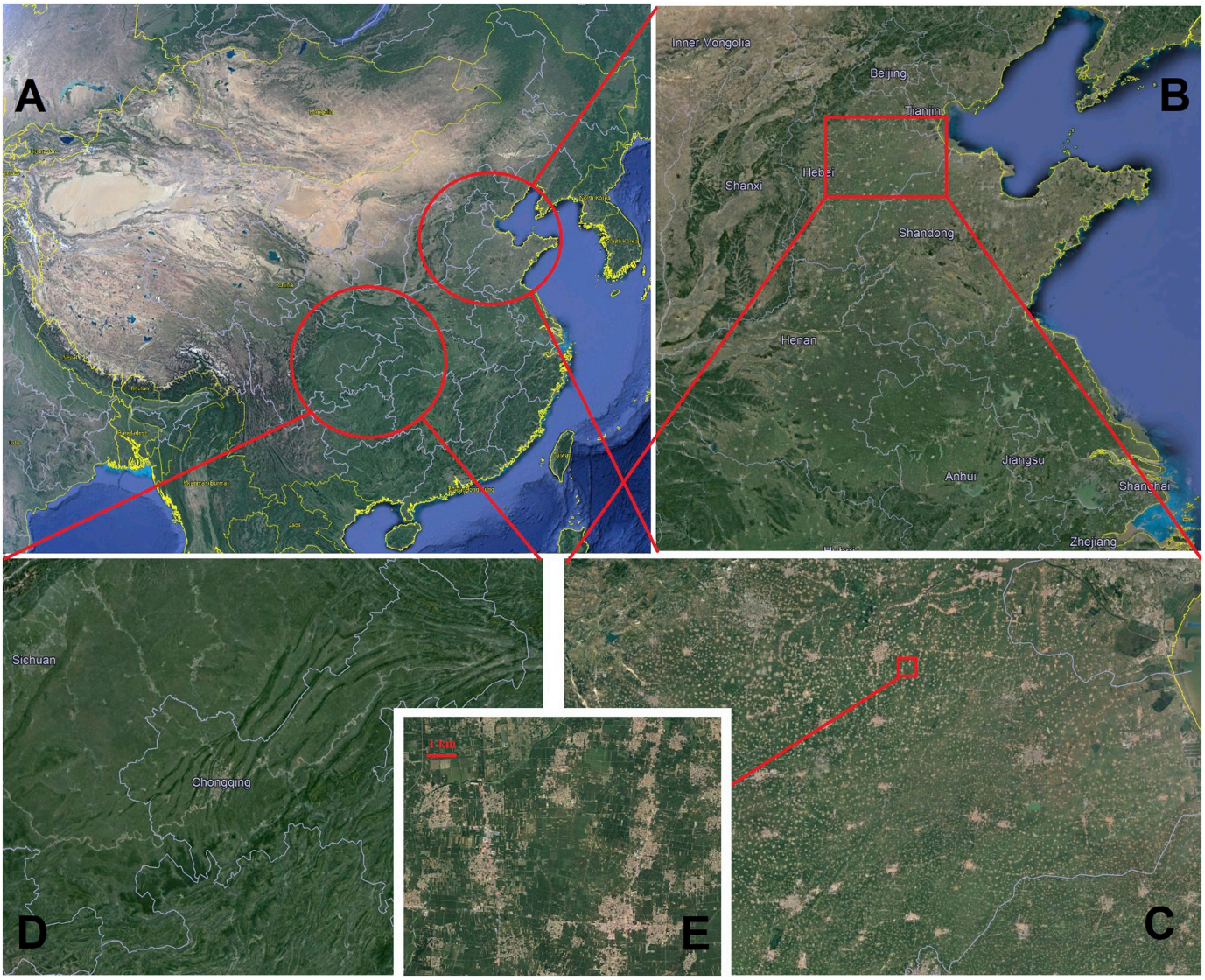

Fig. 13. [A] Google-Pro satellite images of China. [B] Zoom over the North-East region. [C] Farther zoom of the selected region in B. The large bright dots are major cities while the little ones are thousands of small towns as demonstrated in the zoom shown in [E]. [D] Zoom of the green province of Chongqing and the surrounding ones. (For interpretation of the references to colour in this figure legend, the reader is referred to the web version of this article.)

Table 4
Change in mean temperature between 1940–1949, 1970–1979 and 2000–2009 in the CRU TS4.01 temperature records and CMIP5 GCM ensemble mean simulations for the maximum, average and minimum temperature records.

Temp. Anom. 1940–1950	$T_{1970–1979}–T_{1940–1949}$ (°C)	$T_{2000–2009}–T_{1970–1979}$ (°C)	$T_{2000–2009}–T_{1940–1949}$ (°C)
CRU TS4.01 Tmax	−0.53 ± 0.14	0.73 ± 0.14	0.20 ± 0.14
CRU TS4.01 Tmean	−0.31 ± 0.11	0.93 ± 0.11	0.62 ± 0.11
CRU TS4.01 Tmin	−0.10 ± 0.10	1.15 ± 0.10	1.05 ± 0.10
GCMIP5 TS Tmax	−0.11 ± 0.04	0.72 ± 0.04	0.61 ± 0.04
GCMIP5 TS Tmean	−0.07 ± 0.04	0.77 ± 0.04	0.70 ± 0.04
GCMIP5 TS Tmin	−0.04 ± 0.04	0.82 ± 0.04	0.78 ± 0.04

the CMIP5 GCM simulation between the following decades over China: 1) 1970–1979 and 1940–1949; 2) 2000–2009 and 1970–1979; 3) 2000–2009 and 1940–1949. Again, we use a 60-year interval to reduce possible statistical artifacts due to a 60-year climatic oscillation.

The analysis indicates that over China the CRU TS4 temperature decreased from the 1940s to the 1970s. However, while Tmax decreased by about 0.5 °C, Tmin decreased only by about 0.1 °C. From the 1970s to the 2000s the temperature increased. However, Tmax increased by about 0.7 °C while Tmin by 1.1–1.2 °C. Thus, from the 1940s to the 2000s Tmax increased by about 0.2 °C while Tmin increased by

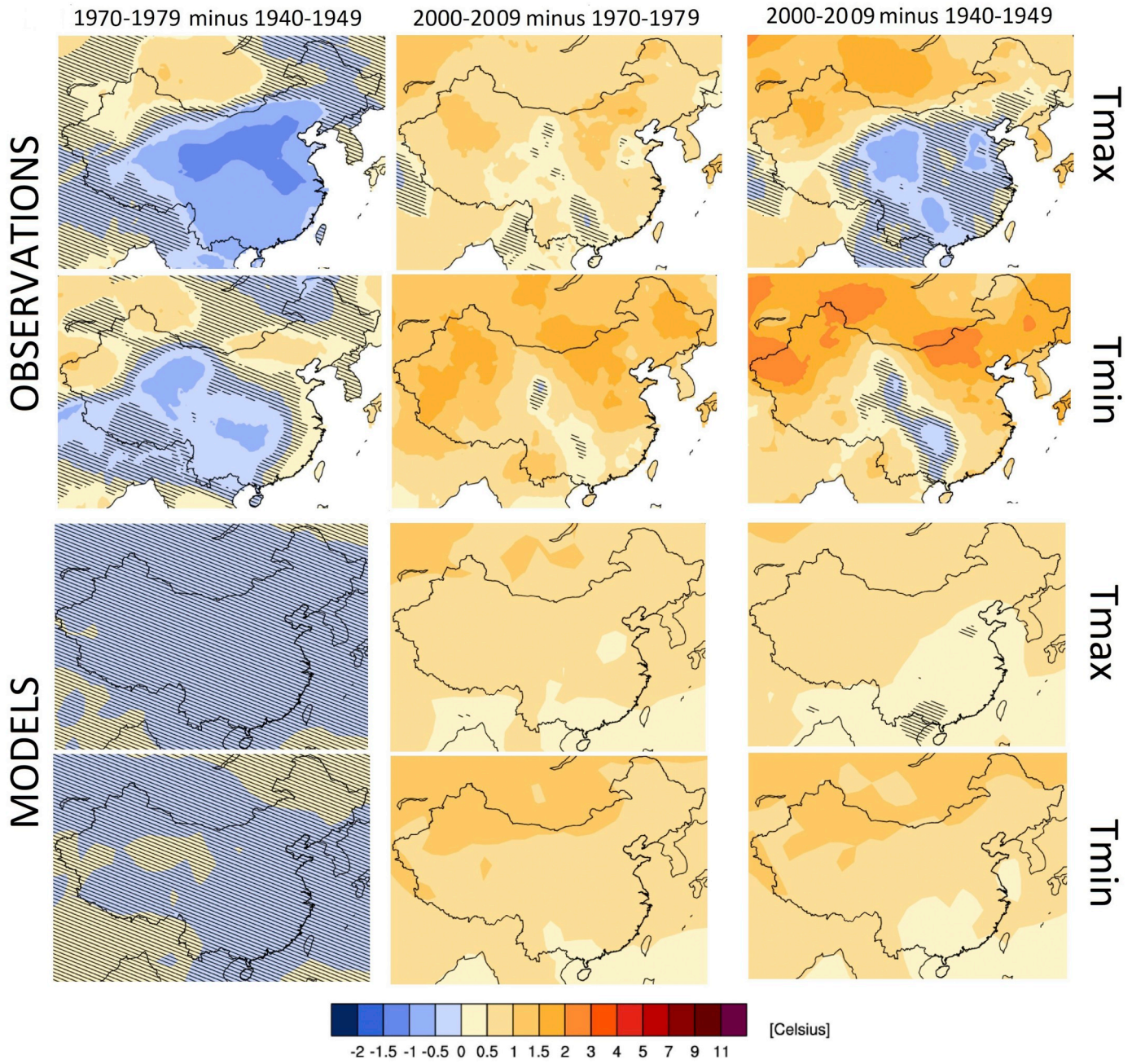

Fig. 14. Maps comparison between observations (CRU TS4) and CMIP5 GCM mean ensemble simulations. Tmax and Tmin variations between: 1970–1979 and 1940–1949; 2000–2009 and 1970–1979; 2000–2009 and 1940–1949. The hatching represents areas where the signal is smaller than one standard deviation of natural variability (e.g. the value is nearly zero).

1.0–1.1 °C. In conclusion, it appears that the current warm period is just slightly warmer than the 1940s warm period when Tmax is considered. On the contrary, using Tmin the current warm period is significantly warmer than the early 20th-century one. The divergence between the two results is about 0.8–0.9 °C.

The significance of this result is highlighted by the comparison against the CMIP5 GCM mean ensemble simulations. Here, Tmin is just slightly warmer than Tmax. From the 1940s to the 1970s Tmax decreased by about 0.11 °C while Tmin decreased by about 0.04 °C. This result is likely a consequence of the leftover cooling induced by the VEI 5 eruption of Mt. Agung (1962) and by other nine VEI 4 eruptions between 1964 and 1976. From the 1970s to the 2000s Tmax increased by about 0.7 °C while Tmin increased by 0.8 °C. Thus, according to the CMIP5 GCMs, from the 1940s to the 2000s Tmax had to increase by about 0.6 °C while Tmin by about 0.8 °C. The difference had to be just about 0.2 °C, which is 4–5 times less than what the CRU TS4 records show.

Fig. 14 shows ΔT_{Min} and ΔT_{Max} maps over China, both for the CRU TS4 record and the CMIP5 GCM simulations between the decades: 1) 1970–1979 and 1940–1949; 2) 2000–2009 and 1970–1979; 3) 2000–2009 and 1940–1949. The maps confirm that from the 1940s to the 1970s Tmax cooled (blue colour) significantly more than Tmin up to

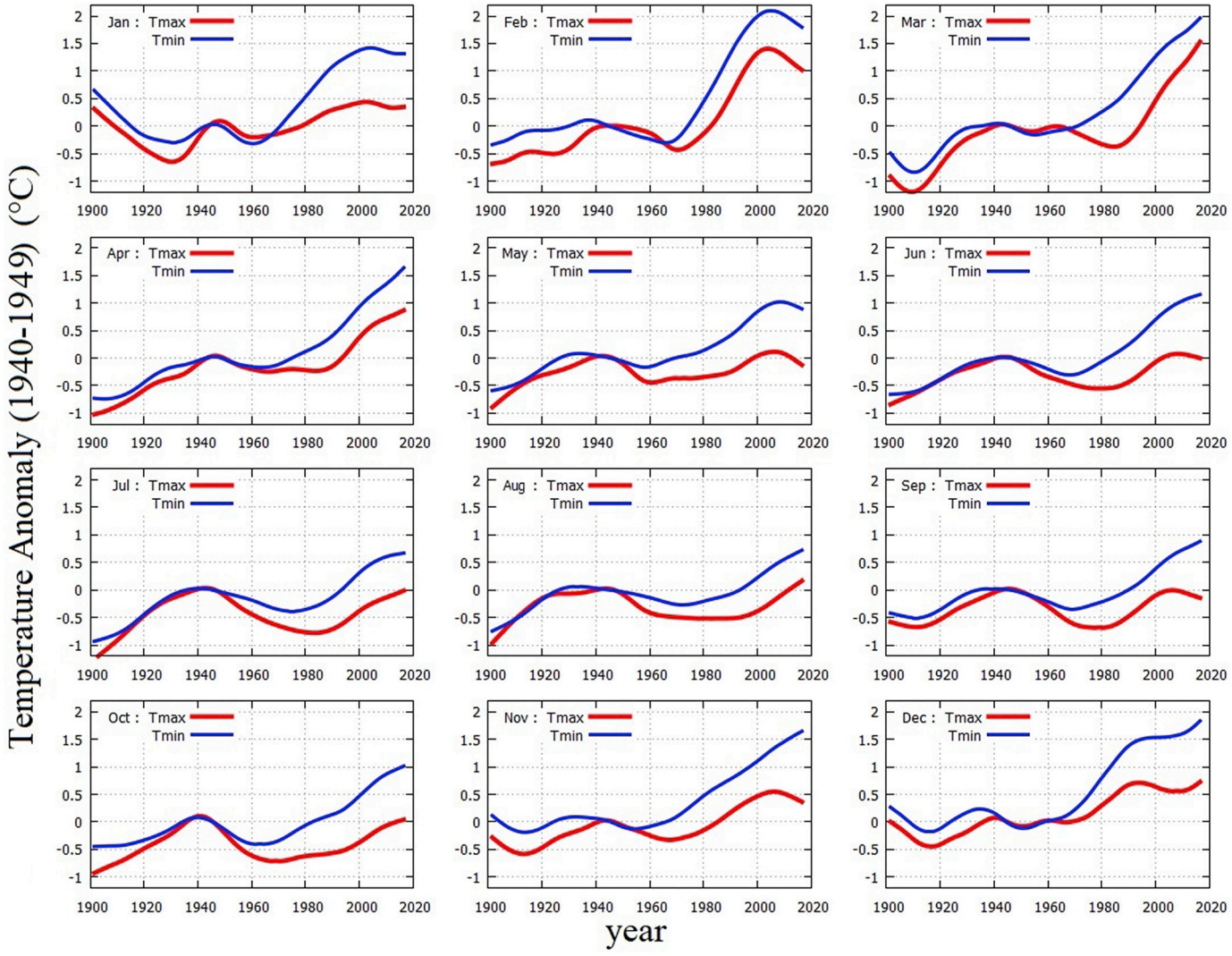

Fig. 15. CRU TS4.01 Tmax (red) and Tmin (blue) records for each month over China smoothed with an acsplines filter: See Table 6. (For interpretation of the references to colour in this figure legend, the reader is referred to the web version of this article.)

Table 5
Changes in Tmax, Tmin and their difference between the periods 1940–1949 and 2000–2009 per month and season.

Period	Observation (°C)			Models (°C)		
	ΔT_{max}	ΔT_{min}	$\Delta T_{min} - \Delta T_{max}$	ΔT_{max}	ΔT_{min}	$\Delta T_{min} - \Delta T_{max}$
Jan	0.08 ± 0.34	1.22 ± 0.20	1.14 ± 0.39	0.70 ± 0.06	0.86 ± 0.05	0.16 ± 0.08
Feb	1.33 ± 0.64	2.04 ± 0.52	0.71 ± 0.82	0.64 ± 0.09	0.81 ± 0.09	0.17 ± 0.13
Mar	0.90 ± 0.26	1.47 ± 0.22	0.57 ± 0.34	0.51 ± 0.07	0.63 ± 0.06	0.12 ± 0.09
Apr	0.33 ± 0.21	1.01 ± 0.14	0.68 ± 0.25	0.70 ± 0.06	0.80 ± 0.06	0.10 ± 0.08
May	0.24 ± 0.22	1.12 ± 0.10	0.88 ± 0.24	0.53 ± 0.04	0.73 ± 0.03	0.20 ± 0.05
Jun	−0.09 ± 0.09	0.87 ± 0.07	0.96 ± 0.11	0.55 ± 0.04	0.74 ± 0.04	0.19 ± 0.06
Jul	−0.31 ± 0.14	0.53 ± 0.10	0.84 ± 0.17	0.45 ± 0.03	0.71 ± 0.03	0.26 ± 0.04
Aug	−0.31 ± 0.16	0.47 ± 0.11	0.78 ± 0.19	0.58 ± 0.03	0.77 ± 0.03	0.19 ± 0.04
Sep	−0.05 ± 0.10	0.64 ± 0.12	0.69 ± 0.16	0.63 ± 0.03	0.83 ± 0.03	0.20 ± 0.04
Oct	−0.35 ± 0.23	0.73 ± 0.20	1.08 ± 0.30	0.62 ± 0.04	0.73 ± 0.05	0.21 ± 0.06
Nov	0.19 ± 0.33	0.97 ± 0.28	0.78 ± 0.43	0.67 ± 0.05	0.79 ± 0.06	0.12 ± 0.08
Dec	0.40 ± 0.28	1.53 ± 0.23	1.13 ± 0.36	0.75 ± 0.05	0.94 ± 0.05	0.19 ± 0.07
Season						
Nov–Apr	0.57 ± 0.20	1.39 ± 0.15	0.82 ± 0.25	0.66 ± 0.04	0.82 ± 0.05	0.16 ± 0.06
May–Oct	−0.14 ± 0.09	0.73 ± 0.07	0.87 ± 0.11	0.56 ± 0.03	0.75 ± 0.03	0.19 ± 0.04

Comparison between CRU TS4.01 observations and CMIP5 GCM ensemble mean simulations.

Table 6
Changes in Tmax, Tmin and their difference between the periods 1940–1949 and 2000–2009 per month and season.

Period	Observation (°C)			Models (°C)		
	ΔT_{max}	ΔT_{min}	$\Delta T_{min} - \Delta T_{max}$	ΔT_{max}	ΔT_{min}	$\Delta T_{min} - \Delta T_{max}$
Jan	0.40 ± 0.01	1.39 ± 0.01	0.99 ± 0.02	0.64 ± 0.05	0.82 ± 0.06	0.18 ± 0.08
Feb	1.36 ± 0.01	2.06 ± 0.01	0.70 ± 0.02	0.54 ± 0.06	0.75 ± 0.06	0.20 ± 0.08
Mar	0.79 ± 0.07	1.49 ± 0.04	0.70 ± 0.08	0.50 ± 0.06	0.66 ± 0.06	0.16 ± 0.08
Apr	0.57 ± 0.04	1.14 ± 0.04	0.57 ± 0.06	0.60 ± 0.06	0.72 ± 0.06	0.12 ± 0.08
May	0.09 ± 0.01	0.96 ± 0.02	0.87 ± 0.02	0.52 ± 0.05	0.7 ± 0.05	0.18 ± 0.07
Jun	0.03 ± 0.02	0.88 ± 0.04	0.85 ± 0.05	0.51 ± 0.05	0.69 ± 0.05	0.18 ± 0.07
Jul	−0.25 ± 0.03	0.48 ± 0.03	0.73 ± 0.05	0.46 ± 0.05	0.68 ± 0.05	0.22 ± 0.07
Aug	−0.23 ± 0.04	0.40 ± 0.04	0.63 ± 0.06	0.57 ± 0.05	0.73 ± 0.05	0.16 ± 0.07
Sep	−0.04 ± 0.01	0.57 ± 0.04	0.61 ± 0.04	0.61 ± 0.06	0.76 ± 0.06	0.15 ± 0.08
Oct	−0.22 ± 0.03	0.68 ± 0.04	0.90 ± 0.05	0.59 ± 0.05	0.72 ± 0.06	0.13 ± 0.08
Nov	0.52 ± 0.01	1.29 ± 0.04	0.77 ± 0.04	0.65 ± 0.05	0.78 ± 0.06	0.12 ± 0.08
Dec	0.58 ± 0.01	1.56 ± 0.01	0.98 ± 0.02	0.74 ± 0.06	0.94 ± 0.07	0.20 ± 0.09
Season						
Nov–Apr	0.72 ± 0.01	1.52 ± 0.02	0.80 ± 0.02	0.62 ± 0.06	0.78 ± 0.06	0.16 ± 0.08
May–Oct	−0.10 ± 0.02	0.66 ± 0.03	0.76 ± 0.04	0.54 ± 0.05	0.71 ± 0.06	0.17 ± 0.08

Comparison between CRU TS4.01 observations and CMIP5 GCM ensemble mean simulations using the smooth curves depicted in Figs. 15, 16, 18 and 19.

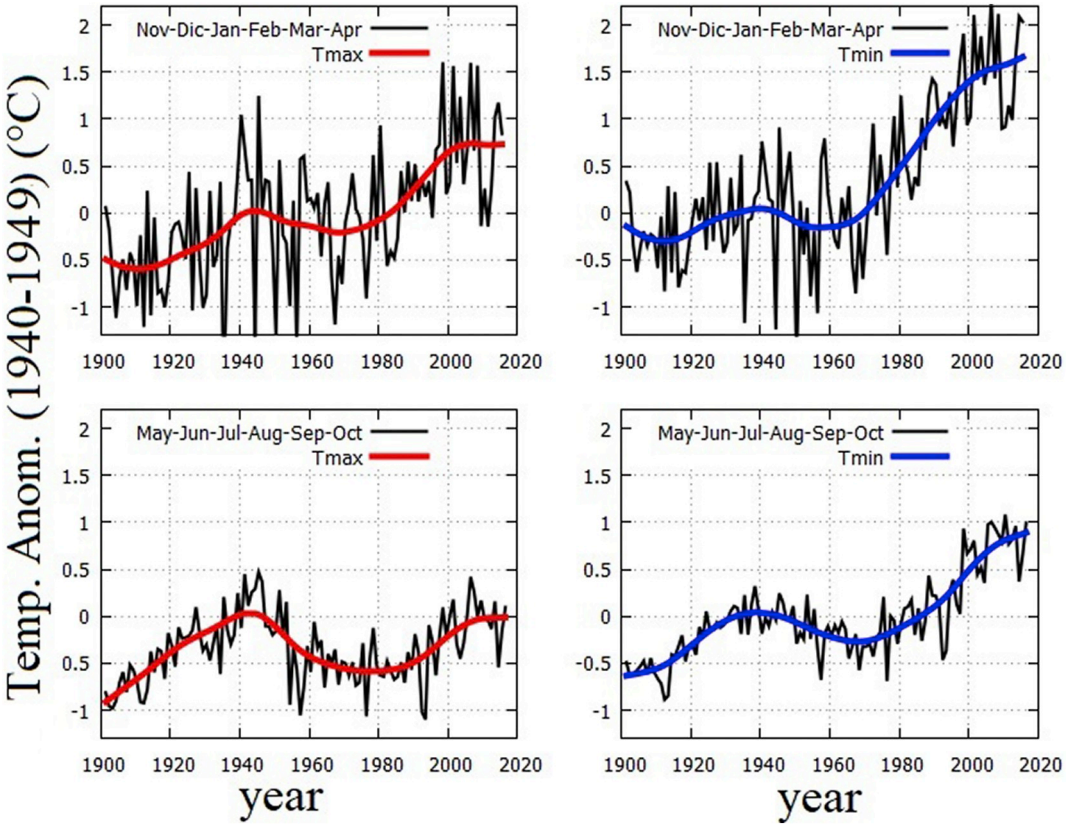

Fig. 16. CRU TS4.01 Tmax (red) and Tmin (blue) records for the 6 coldest months (November–April) and for the 6 warmer months (May–October). Data (black) and their smoothed version (red and blue) with an acsplines filter: See Table 6. (For interpretation of the references to colour in this figure legend, the reader is referred to the web version of this article.)

1.0–1.5 °C over some regions of central China. From the 1970s to the 2000s Tmax was still significantly cooler than Tmin (lighter yellow versus stronger yellow). Finally, in most central and east China, the 2000s Tmax temperature values have been equivalent or even cooler (blue colour) than the 1940s Tmax temperature values. A very different pattern is observed in the CMIP5 ensemble mean simulations. Here Tmin values are just slightly warmer than Tmax ones and the result is quite uniform over China. In both cases, the GCM simulations do not show any significant cooling between the 1940s and the 1970s, which, on the contrary, is quite visible in the CRU observations.

The analysis is now repeated for each month separately to determine whether a seasonal effect is observed. Fig. 15 compares acsplines (the "natural smoothing spline" of Gnuplot using the parameter 0.001: available at http://www.gnuplot.info/) smooth curves of the Tmax and Tmin CRU TS4 records over China for each month relative to the mean period 1940–1949. Table 5 reports the Tmax and Tmin mean

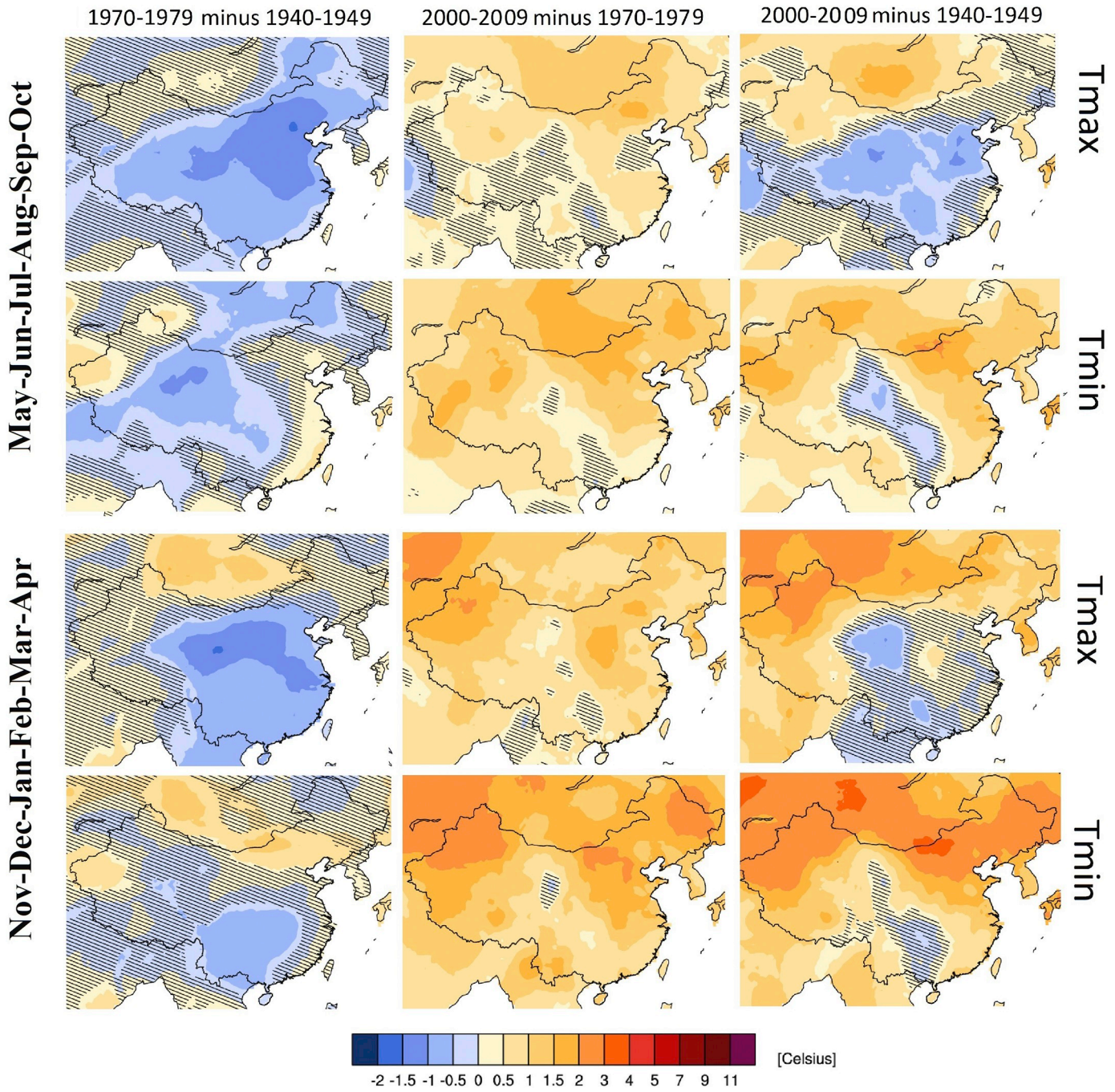

Fig. 17. Tmax and Tmin map distribution comparisons using CRU TS4 records for the 6 coldest months (November–April) and for the 6 warmer months (May–October). Used intervals: 1970–1979 and 1940–1949; 2000–2009 and 1970–1979; 2000–2009 and 1940–1949. The hatching represents areas where the signal is smaller than one standard deviation of natural variability (e.g. the value is nearly zero).

temperature values in the decades 1940–1949 and 2000–2009. Finally, the table reports their difference for each month. Table 6 does the same but now the calculations are performed using the acsplines smooth curves depicted in Fig. 15. This double evaluation was conducted because of the large volatility of these records. The results are statistically compatible and used in our following discussion. Finally, both tables report their difference for each month.

Fig. 15 and Table 6 again show that Tmin records warmed on average by 0.8 ± 0.2 °C significantly more than Tmax. However, now we also observe a seasonal dependency. Both Tmax and Tmin warmed more during the cooler months from November–April than during the warmer months from May to October. This behavior is more evident in Fig. 16 that compares the Tmax and Tmin CRU TS4 mean records over China for the colder months from November–April versus the warmer months from May to October. As reported in Table 6, from 1940–1949 to 2000–2009 Tmax increased by about 0.7 °C during the six colder

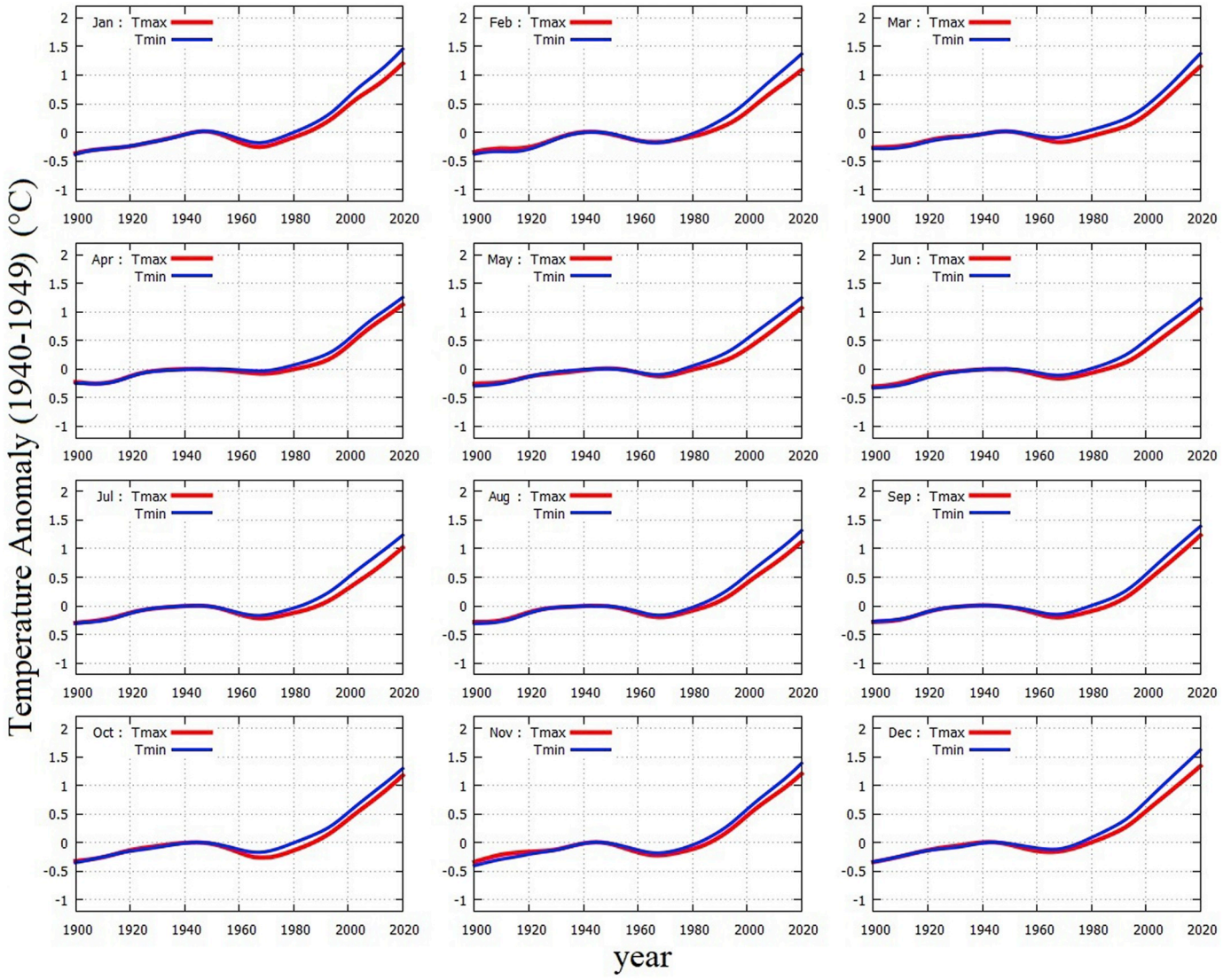

Fig. 18. CMIP5 GCM ensemble mean simulations over China. Tmax (red) and Tmin (blue) records for each month over China. Compare versus Fig. 14. The curves are smoothed with an acsplines filter: See Table 6. (For interpretation of the references to colour in this figure legend, the reader is referred to the web version of this article.)

months while decreased by about 0.1 °C during the six warmer months. During the same periods, Tmin increased by about 1.5 °C during the six colder months and increased by about 0.7 °C during the six warmer months.

Finally, Fig. 17 shows ΔT_{Min} and ΔT_{Max} maps over China for the CRU TS4.01 record for the November–April and May–October for the decades: 1) 1970–1979 and 1940–1949; 2) 2000–2009 and 1970–1979; 3) 2000–2009 and 1940–1949. From the 1940s to the 1970s, during the six warmer months Tmax significantly cooled over nearly the whole of China. Tmin cooled over about 50% of China. During the six cooler months Tmax and Tmin cooled, although less, from the 1940s to the 1970s. On the contrary, from the 1940s to the 2000s, while Tmax cooled during the six warmer months over at least 50% of China, in particular over the central and east areas, Tmin mostly warmed over the whole country. Between the same two periods and during the six colder months Tmax moderately warmed over the whole China while Tmin warmed much more.

The monthly analysis was repeated using the CMIP5 GCM ensemble simulations over China and the results plotted in Figs. 18 and 19. The numerical results reported in Tables 5 and 6 and those referring to the smoothed curves are depicted in Fig. 20. Again, we find that from the 1940s and the 2000s the synthetic Tmin warmed only slightly more than Tmax, by about 0.17 ± 0.03 °C. This is about five times less than what found in the CRU TS4 records. In addition, the CMIP5 GCM simulations show only a modest monthly or seasonal variability between Tmax and Tmin when compared against the clear seasonality shown by the CRU TS4 Tmax and Tmin records: see Fig. 20.

6. Conclusion

This work aims to complement the review proposed by Soon et al. (2015, 2018) regarding the possible persistence of an urbanization bias

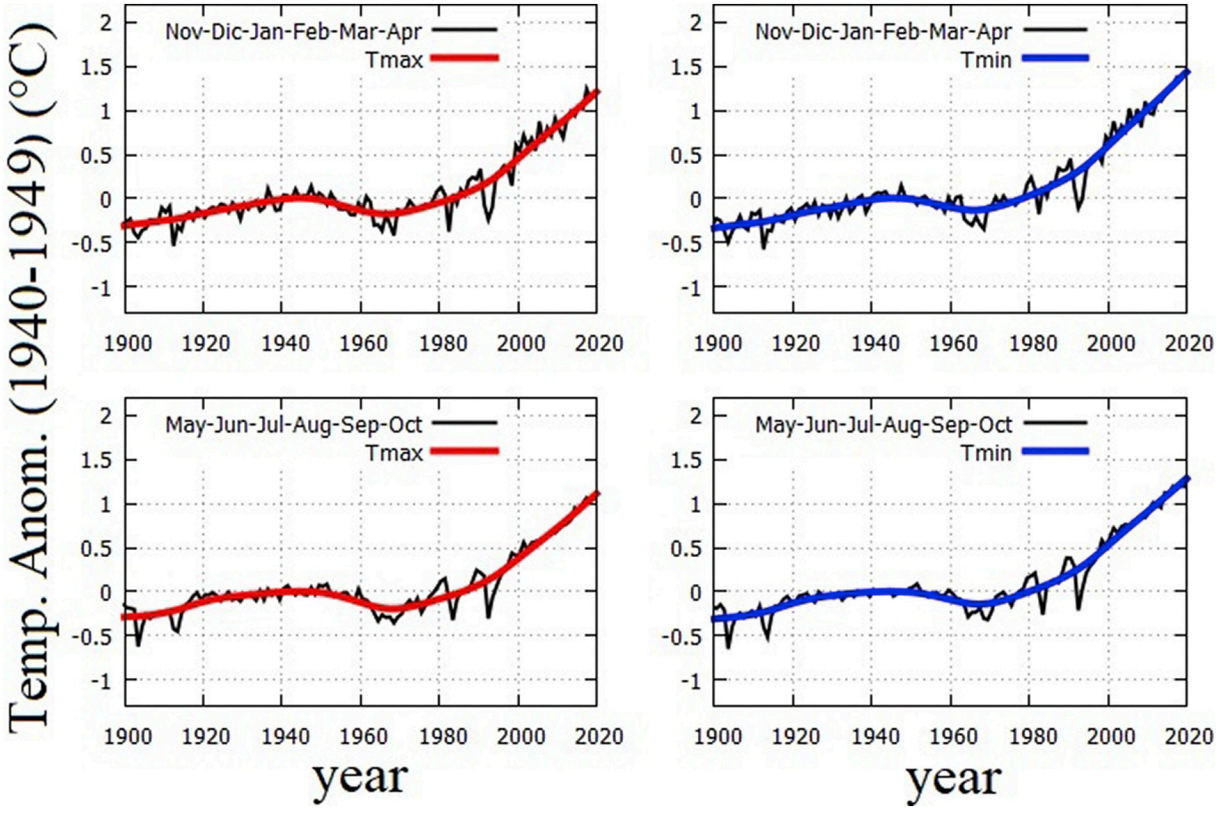

Fig. 19. CMIP5 GCM ensemble mean simulations over China. CRU TS4 Tmax (red) and Tmin (blue) records for the 6 coldest months (November–April) and for the 6 warmer months (May–October). Compare versus Fig. 15. Data (black) and their smoothed version (red and blue) with an acsplines filter: See Table 6. (For interpretation of the references to colour in this figure legend, the reader is referred to the web version of this article.)

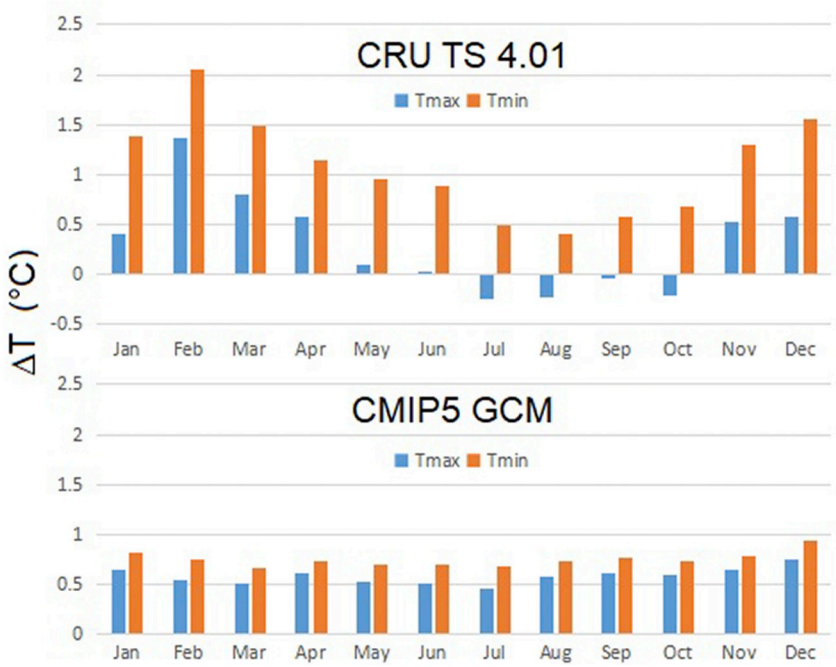

Fig. 20. Changes in Tmax, Tmin and their difference between the periods 1940–1949 and 2000–2009 per month. Comparison between CRU TS4 observations and CMIP5 GCM ensemble mean simulations. See Table 6.

in the available climatic records over China. Our analysis takes into account that the likely best methodology to detect and quantify urbanization biases is by considering the physical properties of the atmospheric boundary layers predicting that UHI effects vary according to season and the time of day (Oke, 1987; Stull, 1988; Kershaw, 2017). Thus, we have studied the available Tmax and Tmin network records over China at the annual and monthly scales. The significance of our results was tested against the predictions of the CMIP5 GCM ensemble mean simulations.

The known atmospheric physics implemented in the CMIP5 GCMs predict that Tmin has to warm slightly more than Tmax over China and for every month. This result may be reasonable because the different behaviors between Tmin and Tmax derive from the physics of atmospheric convection and evaporation that could be sufficiently well modeled. However, it is also true that these models have several problems in actually reproducing the real climate system with its numerous oscillations and patterns (e.g.: Scafetta, 2013a, 2013b). Most of the models' shortcomings are likely related to the type of adopted forcings and the current poor knowledge regarding cloud formation physics (cf.: Bindoff et al., 2013) that make the climate sensitivity to radiative forcing still uncertain today as it was 40 years ago (Knutti et al., 2017).

In any case, our analysis of the CRU TS4 records demonstrates that since the 1940s over vast regions of China Tmin has warmed significantly more than Tmax relative to the GCMs' predictions: see Figs. 6 and 8. The regions where this divergence mostly occurred also coincide with the most densely populated regions of China (more than 400 people/km^2) such as for example the provinces of Bejing, Tianjin, Jiangsu, Shandong, Henan, Anhui and Hebei and in other places that have experienced a widespread and significant urbanization process during the same period: one of the largest in the world. Google-Pro satellite photographs of this region depicted in Fig. 13 demonstrate that, among the large urban centers, these regions do not contain real rural areas because thousands of little towns and villages at about 2 km from each other fill the area. Thus, it is legitimate to conclude that a significant urbanization bias is present in the CRU climate records over China, which could not be filtered out by usual homogenization methods.

Since, as explained in the introduction, UHI effects bias Tmin more than Tmax records, in Section 4 we suggested that between the period 1945–1954 and 2005–2014 China could have experienced at most a warming of 0.46 ± 0.13 °C instead of the reported 0.79 ± 0.10 °C. However, in Section 5 we also noted a significant seasonal dependency of the effect. Indeed, UHI biases not only Tmin but, although more moderately, also Tmax. Because the standard high-pressure weather conditions over China during the cooler months of November–April would strengthen a UHI bias in the temperature records, it is possible to argue that the Tmax record registered during the warmer months of May–October might be more indicative of the real climatic temperature variation over this region. In this case, based on the mean values reported in Table 4, regarding both the CRU TS4 records and the synthetic ones, it is possible that both the current post-2000 and early 20th century (during the 1940s) warm periods in China have been nearly compatible. Relative to the 1940s, the current warm period could have been slightly colder in some regions of China and warmer in others, as Fig. 17 reports.

The fact that the largest observed discrepancies are quite well correlated with the areas that have experienced a high level of urbanization, is a good indication that much of the identified difference is probably due to UHI biases. However, Hubbard and Lin (2006) found that the biases associated with a network-wide 1980s change in instrumentation used in the United States were of opposite sign for Tmax and Tmin. Similarly, Fall et al. (2011) found that poor siting quality leads to a station exposure bias that is greater for Tmin than Tmax. In theory, changes in time of observation could also introduce different biases for Tmin and Tmax (Karl et al., 1986). Thus, part of our results could be due to other homogenization problems present in the CRU records. In any case, if the proposed analysis has identified non-climatic biases in the data, then this is a concern regardless of whether the exact bias is due to UHI, siting bias, instrumental biases, etc. So, in this sense, the analysis is important even if the identified non-climatic biases are not entirely due to urbanization.

Under the hypothesis that Tmax is probably a better metric for studying climatic changes than Tmean or Tmin, as also argued in McNider et al. (2012), in the case of China, our analysis suggests that up to about 50% of the warming reported on the annual scale from the 1940s to the 2000s by the available climatic record could not have been caused by radiative forcing associated to anthropogenic greenhouse gas emissions, as simulated by the CMIP5 GCMs, but by an uncorrected urbanization thermal bias. Using a different metric also Sun et al. (2016) concluded that urbanization has contributed significantly to the warming in China. This percentage would be even larger if the detected seasonal dependency of Tmin and Tmax warming trends is also linked to an urbanization bias. In this regard, we found that for the 6 months between April–October Tmax did not show any warming between the 1940s and the 2000s. This result contradicts significantly the CMIP5 prediction (compare Figs. 16 and 19) and, perhaps, it might be partially due to an unmodelled aerosol bias (Cai et al., 2016), which should cool daytime temperature more than the nighttime ones (Zdunkowski et al., 1976). However, aerosols should cool both Tmax and Tmin, but we found that, while Tmax usually warmed less than the GCM expectrations, Tmin usually warmed more than them. Thus, an unmodelled aerosol bias may have contributed, but cannot explain the observation.

The above results appear consistent with several other recent studies based on instrumentally recorded climatic records that have suggested that the models significantly overestimate the climate sensitivity to radiative forcing by at least a factor of 2 (e.g.: Lindzen and Choi, 2011; Scafetta, 2013a; Lewis and Curry, 2015; Soon et al., 2015; Bates, 2016; Gervais, 2016; and many others; cf. Knutti et al., 2017).

Appendix A. Appendix

Figs. 6–8 investigate the interval between the decades 1945–1954 and 2005–2014. The introduction raised an issue regarding whether the result could be due to the development of the meteorological network in China, which had become more standard after 1950. To test this hypothetical dependency, Fig. 21 shows on the left panels maps of the divergence ($\Delta T_{Min} - \Delta T_{Max}$) registered by the Tmin and Tmax records in the same CRU TS record between [Top] 1955–1964 and 2005–2014, and [Bottom] between 1965 and 1974 and 2005–2014. On the right panels, the same analysis is repeated using the CMIP5 GCMs. The figure qualitatively confirms the results of Figs. 6 and 7 where most of China is shown to present a significant Tmin warming bias (red-dark) relative to Tmax, in particular in the highly densely populated North-East region [112°–120°E:32°–40°N].

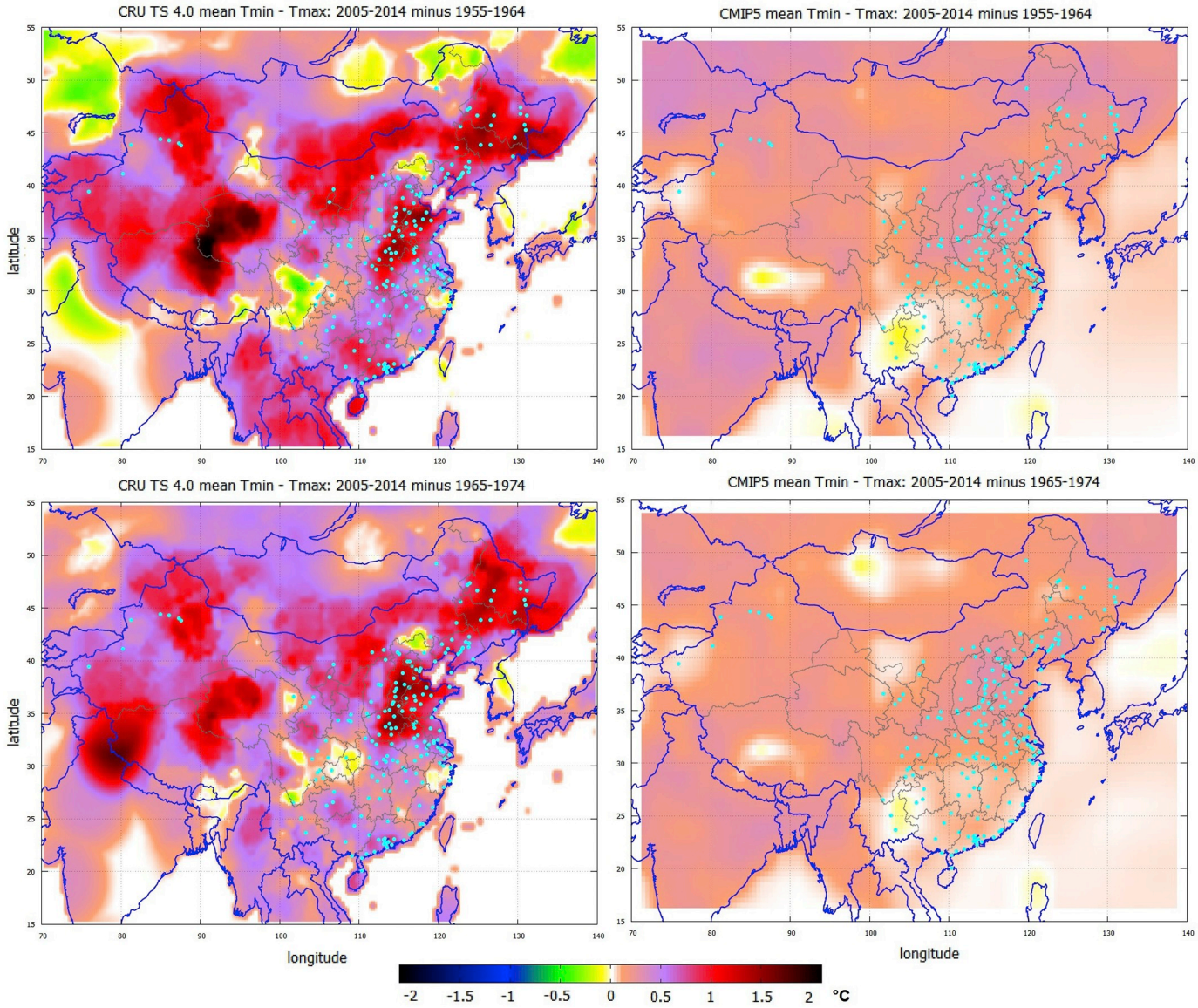

Fig. 21. Map of the divergence ($\Delta T_{Min} - \Delta T_{Max}$) between the warmings registered by the minimum and maximum temperature records (CRU TS4 left, CMIP5 GCM right) between [Top] 1955–1964 and 2005–2014, and [Bottom] 1965–1974 and 2005–2014. The cyan dots indicate the 200 most populated cities in China according to the Free World City Database. (For interpretation of the references to colour in this figure legend, the reader is referred to the web version of this article.)

References

Bates, J.R., 2016. Estimating climate sensitivity using two-zone energy balance models. Earth Space Sci. 3, 207–225.

Bindoff, N.L., Stott, P.A., AchutaRao, K.M., et al., 2013. Detection and attribution of climate change: from global to regional. In: Stocker, T.F. (Ed.), Climate Change 2013: The Physical Science Basis. Contribution of Working Group 1 to the Fifth Assessment Report of the Intergovernmental Panel on Climate Change. Cambridge University Press, Cambridge, UK and New York, NY, USA.

Cai, J., Guan, Z., Ma, F., 2016. Possible combined influences of absorbing aerosols and anomalous atmospheric circulation on summertime diurnal temperature range variation over the middle and lower reaches of the Yangtze River. J. Meteor. Res. 30 (6), 927–943.

Cao, L.J., Zhao, P., Yan, Z.W., et al., 2013. Instrumental temperature series in eastern and Central China back to the nineteenth century. J. Geophys. Res. 118, 8197–8207.

Christiansen, B., Ljungqvist, F.C., 2012. The extra-tropical Northern Hemisphere temperature in the last two millennia: reconstructions of low-frequency variability. Clim. Past 8, 765–786.

de Gaetano, A.T., 2006. Attributes of several methods for detecting discontinuities in mean temperature series. J. Clim. 19, 838–853.

Ding, Y.H., Liu, Y.J., Liang, S.J., et al., 2014. Interdecadal variability of the East Asian Winter Monsoon and its possible links to global climate change. J. Meteor. Res. 28, 693–713.

Fall, S., Watts, A., Nielsen-Gammon, J., et al., 2011. Analysis of the impacts of station exposure on the U.S. Historical Climatology Network temperatures and temperature trends. J. Geophys. Res. 116, D14120.

Gervais, F., 2016. Anthropogenic CO_2 warming challenged by 60-year cycle. Earth Sci. Rev. 155, 129–135.

Harris, I., Jones, P.D., Osborn, T.J., Lister, D.H., 2014. Updated high-resolution grids of monthly climatic observations – the CRU TS3.10 Dataset. Int. J. Climatol. 34, 623–642.

Hartmann, D.L., 2016. Global Physical Climatology, Second edition. Oxford.

Hoyt, D.V., Schatten, K.H., 1993. A discussion of plausible solar irradiance variations, 1700–1992. J. Geophys. Res. 98, 18895–18906.

Hubbard, K.G., Lin, X., 2006. Reexamination of instrument change effects in the U.S. Historical Climatology Network. Geophys. Res. Lett. 33, L15710.

Jones, P., 2016. The reliability of global and hemispheric surface temperature records. Adv. Atmos. Sci. 33 (3), 269–282.

Jones, P.D., Lister, D.H., Osborn, T.J., Harpham, C., Salmon, M., Morice, C.P., 2012. Hemispheric and large-scale land surface air temperature variations: an extensive revision and an update to 2010. J. Geophys. Res. 117, D05127.

Karl, T.R., Williams, C.N., Young, P.J., Wendland, W.M., 1986. A model to estimate the time of observation bias associated with monthly mean maximum, minimum and mean temperatures for the United States. J. Climate Appl. Meteor. 25, 145–160.

Kerr, R.A., 2001. A variable sun paces millennial climate. Science 294, 1431–1433.

Kershaw, T., 2017. The urban heat island (UHI), chap. 4. In: Kershaw, T. (Ed.), Climate Change Resilience in the Urban Environment, London.

Kirkby, J., 2007. Cosmic rays and climate. Surv. Geophys. 28, 333–375.
Knutti, R., Rugenstein, M.A.A., Hegerl, G.C., 2017. Beyond equilibrium climate sensitivity. Nat. Geosci. 10, 727–736.
Lewis, N., Curry, J.A., 2015. The implications for climate sensitivity of AR5 forcing and heat uptake estimates. Clim. Dyn. 45, 1009–1023.
Li, Q., Zhang, H., Liu, X., et al., 2004. Urban heat island effect on annual mean temperature during the last 50 years in China. Theor. Appl. Climatol. 79, 165–174.
Li, Q.X., Li, W., Si, P., et al., 2010. Assessment of surface air warming in Northeast China, with emphasis on the impacts of urbanization. Theor. Appl. Climatol. 99, 469–478.
Li, Q., Zhang, L., Xu, W., et al., 2017. Comparisons of time series of annual mean surface air temperature for China since the 1900s: observations, model simulations and extended reanalysis. Bull. Am. Meteorol. Soc. 98, 699–711.
Lindzen, R.S., Choi, Y.-S., 2011. On the observational determination of climate sensitivity and its implications. Asia-Pacific J. Atmos. Sci. 47, 377–390.
McNider, R.T., Steeneveld, G.J., Holtslag, A.A.M., et al., 2012. Response and sensitivity of the nocturnal boundary layer over land to added longwave radiative forcing. J. Geophys. Res. 117, D14106.
Oke, T.R., 1987. Boundary Layer Climates, Second edition. New York.
Parker, D.E., 2006. A demonstration that large-scale warming is not urban. J. Clim. 19, 2882–2895.
Peterson, T.C., 2003. Assessment of urban versus rural in situ surface temperatures in the contiguous United States: no difference found. J. Clim. 16, 2941–2959.
Pielke Sr., R.A., Davey, C., Niyogi, D., et al., 2007a. Unresolved issues with the assessment of multi-decadal global land surface temperature trends. J. Geophys. Res. 112, D24S08.
Pielke Sr., R.A., Nielsen-Gammon, J., Davey, C., et al., 2007b. Documentation of uncertainties and biases associated with surface temperature measurement sites for climate change assessment. Bull. Am. Meteorol. Soc. 88, 913–928.
Ren, G.Y., 2015. Urbanization as a major driver of urban climate change. Adv. Clim. Chang. Res. 6, 1–6.
Ren, G.Y., Chu, Z.Y., Chen, Z.H., Ren, Y.Y., 2007. Implications of temporal change in urban heat island intensity observed at Beijing and Wuhan stations. Geophys. Res. Lett. 34, L05711.
Ren, G.Y., Ding, Y.H., Zhao, Z.C., et al., 2012. Recent progress in studies of climate change in China. Adv. Atmos. Sci. 29, 958–977.
Ren, G.Y., Ding, Y.H., Tang, G.L., 2017. An overview of mainland China temperature change research. J. Meteor. Res. 31, 3–16.
Scafetta, N., 2012. A shared frequency set between the historical mid-latitude aurora records and the global surface temperature. J. Atmospheric and Solar-Terrestrial Physics 74, 145–163.
Scafetta, N., 2013a. Discussion on climate oscillations: CMIP5 general circulation models versus a semi-empirical harmonic model based on astronomical cycles. Earth Sci. Rev. 126, 321–357.
Scafetta, N., 2013b. Solar and planetary oscillation control on climate change: hind-cast, forecast and a comparison with the CMIP5 GCMS. Chapter in “Mechanisms of Climate Change and the AGW Concept: a critical review”. Energy Environ. 24 (3–4), 455–496.
Scafetta, N., 2014a. Multi-scale dynamical analysis (MSDA) of sea level records versus PDO, AMO, and NAO indexes. Clim. Dyn. 43, 175–192.
Scafetta, N., 2014b. Discussion on the spectral coherence between planetary, solar and climate oscillations: a reply to some critiques. Astrophys. Space Sci. 354, 275–299.
Scafetta, N., Milani, F., Bianchini, A., Ortolani, S., 2016. On the astronomical origin of the Hallstatt oscillation found in radiocarbon and climate records throughout the Holocene. Earth Sci. Rev. 162, 24–43.
Scafetta, N., Mirandola, A., Bianchini, A., 2017a. Natural climate variability, part 1: observations versus the modeled predictions. Int. J. Heat Technol. 35 (Special Issue 1), S9–S17.
Scafetta, N., Mirandola, A., Bianchini, A., 2017b. Natural climate variability, part 2: interpretation of the post 2000 temperature standstill. Int. J. Heat Technol. 35 (Special Issue 1), S18–S26.
Shi, Z., Jia, G., Hu, Y., et al., 2019. The contribution of intensified urbanization effects on surface warming trends in China. Theor. Appl. Climatol. https://doi.org/10.1007/s00704-019-02892-y.
Soon, W., Connolly, R., Connolly, M., 2015. Re-evaluating the role of solar variability on Northern Hemisphere temperature trends since the 19th century. Earth Sci. Rev. 150, 409–452.
Soon, W.W.-H., Connolly, R., Connolly, M., O'Neill, P., Zheng, J., Ge, Q., Hao, Z., Yan, H., 2018. Comparing the current and early 20th century warm periods in China. Earth Sci. Rev. 185, 80–101.
Stewart, I.D., Oke, T.R., 2012. Local climate zones for urban temperature studies. Bull. Amer. Met. Soc. 93, 1879–1900.
Stull, R.B., 1988. An Introduction to Boundary Layer Meteorology, London.
Sun, Y., Zhang, X., Ren, G., et al., 2016. Contribution of urbanization to warming in China. Nat. Clim. Chang. 6, 706–709.
Tang, G.L., Ren, G.Y., 2005. Reanalysis of surface air temperature change of the last 100 years over China. Clim. Environ. Res. 10, 791–798.
Tang, G.L., Ding, Y.H., Wang, S.W., et al., 2010. Comparative analysis of China surface air temperature series for the past 100 years. Adv. Clim. Chang. Res. 1, 11–19.
Wang, L., Chen, L., 2016. Spatiotemporal dataset on Chinese population distribution and its driving factors from 1949 to 2013. Sci. Data 3, 160047.
Wang, S.W., Gong, D.Y., Zhu, J.H., 2001. Twentieth-century climatic warming in China in the context of the Holocene. Holocene 11, 313–321.
Wang, S.W., Zhu, J.H., Cai, J.N., 2004. Interdecadal variability of temperature and precipitation in China since 1880. Adv. Atmos. Sci. 21, 307–313.
Wang, J., Yan, Z.W., Zhen, L., et al., 2013. Impact of urbanization on changes in temperature extremes in Beijing during 1978–2008. Chin. Sci. Bull. 58, 4679–4686.
Wang, J.F., Xu, C.D., Hu, M.G., et al., 2014. A new estimate of the China temperature anomaly series and uncertainty assessment in 1900–2006. J. Geophys. Res. Atmos. 119, 1–9.
Wang, J., Tett, S.F.B., Yan, Z., 2017. Correcting urban bias in large-scale temperature records in China, 1980–2009. Geophys. Res. Lett. 44, 401–408.
Wyatt, M., Curry, J., 2014. Role of Eurasian Arctic shelf sea ice in a secularly varying hemispheric climate signal during the twentieth century. Clim. Dyn. 42, 2763–2782.
Yan, Z.-W., Wang, J., Xia, J.-J., et al., 2016. Review of recent studies of the climatic effects of urbanization in China. Adv. Clim. Chang. Res. 7, 154–168.
Yang, Y.J., Wu, B.W., Shi, C.E., et al., 2013. Impacts of urbanization and station-relocation on surface air temperature series in Anhui province, China. Pure Appl. Geophys. 170, 1969–1983.
Zhang, L., Ren, G.Y., Ren, Y.Y., et al., 2014. Effect of data homogenization on estimate of temperature trend: a case of Huairou station in Beijing municipality. Theor. Appl. Climatol. 115, 365–373.
Zhao, D., Wu, J., 2019. Comparisons of urban-related warming in Beijing using different methods to calculate the daily mean temperature. Sci. China Earth Sci. 62, 693–702.
Zdunkowski, W.G., Welch, R.M., Paegle, J., 1976. One dimensional numerical simulation of the effects of air pollution on the planetary boundary layer. J. Atmos. Sci. 33, 2399–2414.